MODELLING PYRAZINE AND TETRAZINE COMPLEX IONS OF IRON BY DFT

by

Pınar Ünan

B.S. in Chemistry, Boğaziçi University, 2007

Submitted to the Institute for Graduate Studies in
Science and Engineering in partial fulfillment of
the requirements for the degree of
Master of Science

Graduate Program in Chemistry
Boğaziçi University

2007

ACKNOWLEDGMENTS

Completing a thesis is truly a marathon event, and I would not have been able to complete this work without the aid and support of countless people. I must first express my gratitude to my thesis supervisor Prof. Dr. Tereza Varnalı, for her, understanding, patience, leadership, support, attention to details, hard work, encouragement and guidance throughout this work. She provided me with direction, technical support. Her ideas and tremendous support had a major influence on this thesis. She spend a lot of time helping me. And also I would like to thank Prof. Dr. Tereza Varnalı for giving me the opportunity to work with her.

I would like to thank Prof. Dr. Yüksel İnel and Assis. Prof. Dr. A. Neren Ökte for their rewiew of the final manuscript and all members of the Chemistry Department especially Hülya Metiner for their support.

Last but not least, a very special thanks goes to my family without whose motivation and encouragement. Without their support, none of this work would have been possible and I would not have considered a graduate career in chemistry. Their love and support during long nights of work away at home was of immeasurable value to me.

This work has been supported by B.Ü.Research Funds Project No: 06B507

ABSTRACT

MODELLING PYRAZINE AND TETRAZINE COMPLEX IONS OF IRON BY DFT

In coordination chemistry, mixed valency is widespread, from superconductors to minerals, magnetic molecular clusters and even enzymes. Mixed valency occurs when the same chemical element is found in two different oxidation states in the same molecule or solid.

After the detailed structure and electronic analysis of the ligands tetrazine(tz) and pyrazine(pyz) the metal framework of iron with CN co-ligands, in a progressive manner, mononuclear $[(L)Fe(CN)_5]^{-2,-3}$ (L:tz, pyz), dinuclear $[(\mu\text{-}L)\{Fe(CN)_5\}_2]^{-4,-5}$ complexes and trinuclear trans/cis $[Fe(CN)_5(L)Fe(CN)_4(L)Fe(CN)_5]^{-5,-6,-7}$ complexes are optimized. Some studies on the mononuclear complex (mnc) and mixed valent dinuclear complex (dnc) of Fe in the literature exist but none on tnc complexes. These complexes have been modeled making use of B3LYP (Becke-3-parameters-Lee-Yang-Parr functional) calculations. Comparison of bond lengths, Muliken charges, frontier orbitals, and spins of odd electron species at each level allows a close look at the presence of metal ligand charge transfer (MLCT) and/or intervalence charge transfer (IVCT) of pyrazine and tetrazine iron complexes.

ÖZET

DFT YÖNTEMİ İLE PİRAZİN VE TETRAZİN DEMİR KOMPLEKSLERİNİN MODELLENMESİ

Karışık değerlikli komplekslerin kimyada bir çok kullanım alanı bulunmaktadır. Bunlara süper iletkenlerden minerallere, manyetik molekül gruplarından enzimlere kadar örnek verilebilir. Karışık değerlikli kompleksler, aynı elementin aynı molekülde veya katı maddede farklı oksidasyon basamaklarında bulunması ile gerçekleşir.

Tetrazin, pirazin ve Fe-CN ile birlikte oluşan metal iskeletin kapsamlı olarak yapı ve elektronik analizleri yapıldıktan sonra deneysel verileri literatürde bulunan mononükleer $[(L)Fe(CN)_5]^{-2,-3}$ (L:tz, pyz), ve dinükleer $[(\mu\text{-}L)\{Fe(CN)_5\}_2]^{-4,-5}$ kompleksleriyle deneysel verileri literatürde bulunmayan trans/cis $[Fe(CN)_5(L)Fe(CN)_4(L)Fe(CN)_5]^{-5,-6,-7}$ trinükleer kompleksleri optimize edilmiştir. Bu kompleksler B3LYP (Becke-3-parametresi-Lee-Yang-Parr fonksiyonu) hesaplamaları kullanılarak modellenmiştir. Bağ uzunlukları, Mulliken yükleri, moleküler orbitalleri ve spinlerinin karşılaştırılması ile pirazin ve tetrazin demir komplekslerinin, metal ile ligandın üzerindeki elektronik dağılımından etkileşimine ve iç değerlik yük transferi oluşumuna açıklık getirilmeye çalışılmıştır.

TABLE OF CONTENTS

LIST OF FIGURES

LIST OF TABLES

LIST OF SYMBOLS/ABBREVIATIONS

Å	Angstrom
aHOMO	Alpha highest occupied molecular orbital
aLUMO	Alpha lowest unoccupied molecular orbital
bHOMO	Beta highest occupied molecular orbital
bLUMO	Beta lowest unoccupied molecular orbital
B3LYP	Becke-3-parameter Lee-Yang-Parr functional
bpy	4,4'-bipyridine
bpe	1,2-bis(4-pyridyl)ethylene
bpm	2,2'-bipyrimidine
bmtz	3,6-bis(2-pyrimidyl)-1,2,4,5-tetrazine
bptz	Bis pyridyl tetrazine
C	Carbon
CT	Creutz-Taube Ion
DFT	Density functional theory
dnc	Dinuclear complex
dpp	2,3-bis(2-pyridyl)pyrazine
eV	Electron volt
Fe	Iron
HOMO	Highest occupied molecular orbital
K_c	Comproportionation constant
LUMO	Lowest unoccupied molecular orbital
MO	Molecular orbital
mnc	Mononuclear complex
mndl	Mononuclear diligand
N	Nitrogen
pyz	Pyrazine
tz	Tetrazine
tnc	Trinuclear complex

1. INTRODUCTION

"Mixed valency" describes compounds/complexes which have ions of the same element in two different states of oxidation. Mixed-valence compounds with two or more metal centers in similar or identical settings have become interesting because of their role in biochemistry ($Fe_n^{II, III}$, $Mn_n^{II, III, IV}$, $Cu_2^{I, II}$) [1], their model character for intra molecular electron-transfer reactivity [2], their special spectroscopic or magnetic properties, their potential in 'molecular electronics' and their function as test systems for theoretical approaches.[3] These compounds are perfect candidates for the study of intra molecular electron and energy transfer in both homonuclear and heteronuclear systems. Density functional theory (DFT) was used to study ground and excited state properties of Creutz-Taube (CT) ion.[4,18]

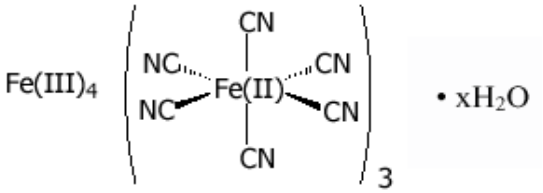

Figure 1.1. Prussian blue

The oldest and most familiar mixed-valent compound, formulated as ferric ferrocyanide [5], Prussian blue (also called Berlin blue) was discovered by accident by the painter Diesbach in Berlin in 1704 (Figure 1.1). [3]

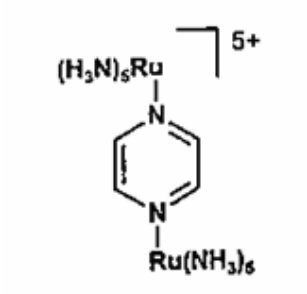

Figure 1.2. Creutz-Taube ion

Another prominent mixed-valent complex is the dnc CT ion (Figure 1.2) which has been extensively studied both experimentally and theoretically since the 1970s [2,6,7]. It is a stable ion. On the vibrational time scale of about 10^{-13}s, the Creutz-Taube ion appears to be a delocalized species with an oxidation number of $^{+}2{,}5$ for both metal centers. [3]

A series of ligand-bridged iron-cyano complexes have been prepared by ligands, L:4,4-bipyridine(bpy) and trans–1,2-bis(4-pyridyl) ethylene (bpe). (Figure 1.3). The spectroscopic and spectroelectrochemical properties of the various combinations of oxidation states of iron have been studied. A strikingly anologous behavior has been found for the $Fe^{II}(CN)_5$ (iron-cyano complex) unit having the same low spin t_{2g} configuration as $Ru^{II}(NH_3)_5$ (ruthenium-ammine complex), The Creutz Taube (CT) ion [8,9]. The mixed-valence iron-cyano complexes have been found to represent examples of weak coupling, belonging to class II of Robin-Day classification [10].

bpe bpy

Figure 1.3. Structure of trans-1,2-bis(4-pyridyl)ethylene (bpe) and 4,4-bipyridine (bpy) complexes

Robin and Day have divided mixed-valence compounds into three different classes;

Class I: Class I complexes are localized and have a very large barrier to electron transfer between the different valences with a slow rate of transfer.

Class III: Class III- complexes are delocalized with no barrier to electron transfer and ultra fast rates.

Class II **:** Class II complexes have properties intermediate to these [12].

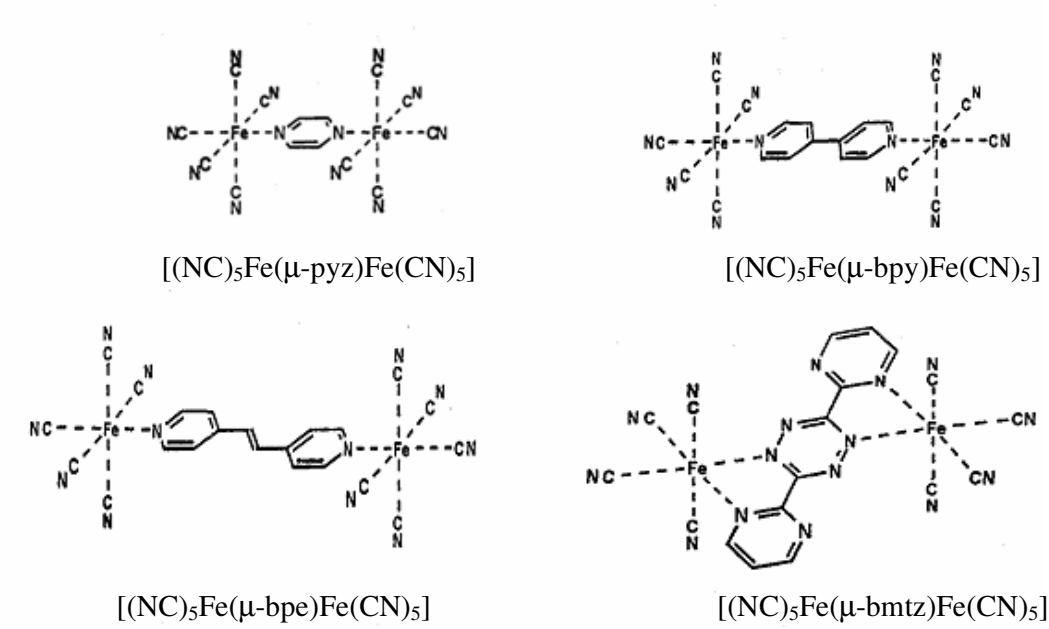

$[(NC)_5Fe(\mu\text{-pyz})Fe(CN)_5]$ $[(NC)_5Fe(\mu\text{-bpy})Fe(CN)_5]$

$[(NC)_5Fe(\mu\text{-bpe})Fe(CN)_5]$ $[(NC)_5Fe(\mu\text{-bmtz})Fe(CN)_5]$

Figure 1.4.Structure of $[(NC)_5Fe(\mu\text{-L})Fe(CN)_5]$ with L:pyz, bpy, bpe and $[(NC)_4Fe(\mu\text{-bmtz})Fe(CN)_4]$ complexes

Similar redox systems (Figure 1.4) were studied in acetonitrile, and other aprotic solvents: such as propylene carbonate or nitromethane. The results illustrate how the established strong solvent sensitivity of cyano iron complexes can be exploited in mixed valence chemistry [11].

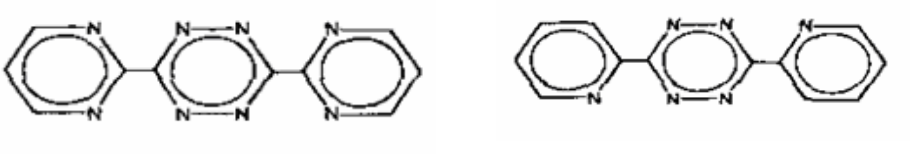

bmtz bptz

Figure 1.5. Structures of bmtz and bptz complexes

Compounds with less effectively bridging ligands [13] (Figure 1.5) in terms of mediating metal-metal interaction were studied. The results on systems bmtz and bptz illustrate clearly that smaller metal-metal distances do not necessarily imply stronger metal-metal interaction. Despite the smaller size of the π system and the shorter metal-metal distance in corresponding dinuclear compounds bpy (Figure 1.3) bridging ligand induces a localized valence situation and a much smaller comproportionation constant (Kc) value than the tetrazines [14].

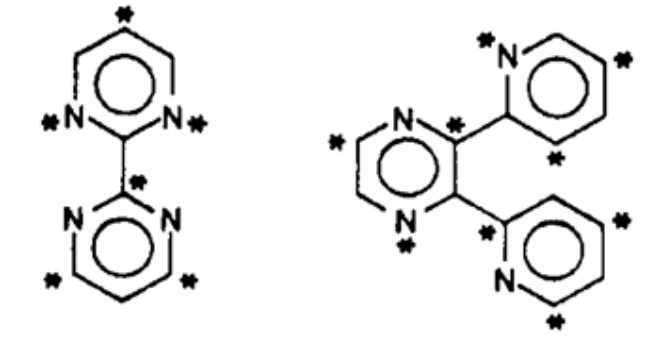

bpm dpp

Figure 1.6. Structure of 2,2'-bipyrimidine and 2,3-bis(2-pyridyl)pyrazine complexes

In small metal systems such as first-row transition metals which are bridged through bpm the use of metals with sterically bulky ligands causes synthesis of useful polymetallic systems to be somewhat difficult. For this reason they have investigated another bridging ligand (dpp), which separates the metal centers more effectively while still providing good communication between metal centers [15]. Richardson and Taube have noted that if a metal is bound to a starred position of an alternating hydrocarbon, the

strongest metal-metal interaction is observed if the second metal is bound to an unstarred position (Figure 1.6) [16].

Glockle et.al. synthesized $[Fe(CN)_5(tz)Fe(CN)_5)]^{-4,-5,-6}$ (Figure 1.7) as a stable species. Also the mono nuclear complex (Figure 1.7) was prepared for comparison purposes. The facile synthesis, high stability, and easy handling correlate with enormous increase in K_c , on going from the pyz to the tz-bridged system. Bis (pentacyanoiron) complex $[(\mu\text{-pyz})Fe(CN)_5]^{5-}$ with pyrazine was found to exhibit only a small K_c ($10^{1.9}$), signifying very little metal-metal interaction.[17]

$Fe(CN)_5(tz)Fe(CN)_5)$ $(\mu\text{-tz})Fe(CN)_5)$

Figure 1.7. Structure of $Fe(CN)_5(tz)Fe(CN)_5)$ and $(\mu\text{-tz})Fe(CN)_5$ complex

There exists experimental studies on mononuclear, dinuclear Fe complexes of tetrazine and pyrazine and similar bridging ligand in the literature[1-8]. Very few modeling studies on these complexes are present also but no study on trinuclear complexes of tetrazine and pyrazine have been encountered. The aim of this work is to study in detail the mixed valent cyanoiron complexes bridged through tetrazine and pyrazine ligands systematically from the mono to the trinuclear complexes. The work starts with detailed structure and electronic analysis of the ligands tetrazine and pyrazine, the metal framework of iron with CN co-ligands, in a progressive manner, mononuclear, dinuclear complexes are followed by the trinuclear complexes. Comparison of bond lengths, frontier orbitals, charges and spins of odd electron species at each level allows a close look at the presence of metal ligand charge transfer (MLCT) and/or intervalence charge transfer (IVCT).

2. COMPUTATIONS

All the computations have been carried out by using the program package SPARTAN'04. [19] Found to be a suitable approach in literature [20], density functional theory (DFT) has been employed.

The DFT functional used is the Becke 3-parameter-Lee-Yang-Parr exchange-correlation functional (B3LYP) [21,22]. This functional was successfully applied to the metals of interest in the literature [23]. B3LYP has been shown to perform well with many difficult chemical problems, including open-shell transition metal chemistry.

In the present study, the 6-31G** basis set is used. In most applications, 6-31G Gaussian basis sets developed by Pople and coworkers are augmented by polarization functions, i.e., functions of higher angular momentum than those occupied in the atom, e.g., p-functions for hydrogen or d-functions for the first-row elements [24].

All the structures were fully geometry optimized with B3LYP/6-31G** methodology. Ground state electronic calculation on all the structures with paired electrons were restricted, whereas for structures with odd number of electrons were unrestricted.

Surface diagrams for the spins of the unpaired electron were drawn to display the spin distribution of structures mononuclear complex (-2), dinuclear complex (-5), trinuclear complex (-5) and trinuclear complex (-7).

Surfaces for the frontier orbitals were drawn to understand the bonding schemes for all the structures.

Mulliken charges on metal frames and the ligands were computed to quantify the charge distribution for all complexes.

3. RESULTS AND DISCUSSION

3.1. METAL FRAMEWORK

To characterize the geometrical changes upon one electron reduction of the metal frameworks in the $[L\text{-}Fe(CN)_5]^{2-,3-}$ complexes (L=tz, pyz) and $[Fe(CN)_6]^{3-,4-}$ complexes (Figure 3.1) were optimized. Their bond lengths are given in Table 3.1.

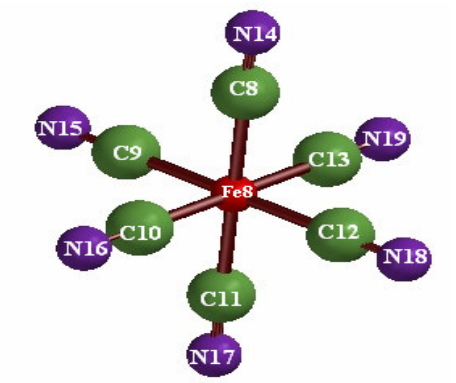

Figure 3.1- Structure and numbering of $[Fe(CN)_6]^{3-,4-}$ complexes

Table 3.1. Bond lengths (Å) for $[Fe(CN)_6]^{3-,4-}$ complexes

BOND	$[Fe(CN)_6]^{3-}$	$[Fe(CN)_6]^{4-}$
Fe7-C8	1.989	2.007
Fe7-C9	1.988	2.007
Fe7-C10	1.981	2.007
Fe7-C11	1.988	2.007
Fe7-C12	1.988	2.007
Fe7-C13	1.981	2.007
C8-N14	1.174	1.184
C9-N15	1.174	1.184
C10-N16	1.175	1.184
C11-N17	1.174	1.184
C12-N18	1.174	1.184
C13-N19	1.175	1.184

$[Fe(CN)_6]^{3-}$ complex has Fe-C bonds 1.988 Å (4 of them in the same plane) and 1.981 Å (the remaining perpendicular two). The C-N bonds are 1.174 Å (four of them in the same plane) and 1.175 Å (the remaining two). Upon one electron reduction all Fe-C bonds lengthen to 2.007 Å and all C-N bonds lengthen to 1.184 Å for $[Fe(CN)_6]^{4-}$ complexes.

3.2. LIGANDS TETRAZINE AND PYRAZINE

The ligands tetrazine (tz) and pyrazine (pyz) were optimized and characterized structurally as well as electronically. The parameters obtained are used for comparison with further calculation results obtained from complexes.

Tetrazine and pyrazine are isoelectronic with 42 electrons (Figure 3.2). Their HOMO (MO index 21) has lone pair character. Their HOMO energies are almost the same (pyz (-6.83 eV), tz (-6.81eV)). LUMO, LUMO(+1) and LUMO(+2) for both of them show π character.

tetrazine pyrazine

Figure 3.2. Structure and numbering of terazine and pyrazine complexes

Tetrazine's LUMO has π* character over the N-N bonds and LUMO(+1) has π* character over the C-N bonds and π character over the N-N bonds (Figure 3.3).

Figure 3.3. LUMO and LUMO(+1) of tetrazine complex

While the LUMO of pyrazine shows π^* character over C-N bonds, over the C-C bonds π character is observed (Figure 3.4).

Figure 3.4. LUMO and LUMO(+1) of pyrazine complex

It is interesting to note that shape of LUMO of tetrazine and LUMO(+1) of pyrazine resemble each other. Similarly shape of LUMO of pyrazine and LUMO(+1) of tetrazine resemble each other.

The LUMO of tetrazine (-3.145 eV) (Figure 3.3) is lower than that of pyrazine (-1.429 eV) and the HOMO-LUMO difference is lower for tz (-5.40 eV for pyz compared to -3.67eV for tz).

To understand the geometrical changes upon one electron reduction, the anions of the ligands have also been optimized.

A comparison of tetrazine and tetrazine anion bond lengths (Table 3.2) show that N1-N2 and N4-N5 bonds lengthen while N1-C6, N2-C3, N5-C6 and C3-N4 bonds shorten slightly. N1 to N4 distance increases by 0.073 Å. These show the one electron reduction consequences for the geometry of tetrazine ring.

Table 3.2. Bond lengths (Å) for tetrazine and tetrazine anion

BOND	Tetrazine	Tetrazine anion
N1-N2	1.325	1.413
N1-C6	1.339	1.333
N2-C3	1.339	1.333
N5-C6	1.339	1.333
C3-N4	1.339	1.333
N4-N5	1.325	1.413
N1-N4	2.735	2.808

Similarly pyrazine and its anion have been optimized. Comparison of pyrazine and pyrazine anion bond lengths (Table 3.3) show that N1-C2, N1-C6, C3-N4 and N4-C5 bonds lengthen and C2-C3 and C5-C6 shorten. N1 to N4 distance increases by 0.144 Å. The pyrazine ring undergoes similar changes as those for tetrazine under one electron reduction.

Table 3.3. Bond lengths (Å) for pyrazine and pyrazine anion

BOND	Pyrazine	Pyrazine anion
N1-C2	1.338	1.383
N1-C6	1.338	1.383
C2-C3	1.396	1.374
C5-C6	1.396	1.374
C3-N4	1.338	1.383
N4-C5	1.338	1.383
N1-N4	2.819	2.963

3.3. TETRAZINE COMPLEXES

3.3.1. MONO NUCLEAR COMPLEXES OF TETRAZINE

The mononuclear complexes $[tz\text{-}Fe(CN)_5]^{2-,\ 3-}$, (tz-mnc(-2), tz-mnc(-3)), have been optimized (Figure 3.5). The bond lengths for each are presented in Table 3.4.

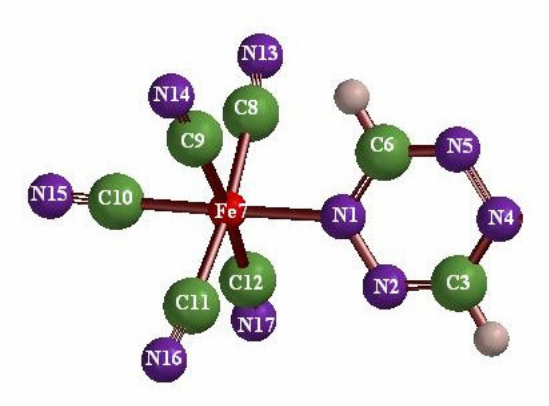

Figure 3.5. Structure and numbering of tetrazine mononuclear complex

Table 3.4. Bond lengths (Å) for tz-mnc(-2) and tz-mnc(-3)complexes

BOND	tz-mnc(-2)	tz-mnc(-3)
N1-N2	1.331	1.387
N1-C6	1.364	1.362
N2-C3	1.335	1.310
N5-C6	1.321	1.327
N4-C3	1.332	1.378
N4-N5	1.350	1.334
N1-N4	2.748	2.804
N1-Fe7	1.967	1.872
Fe7-C8	1.959	1.984
Fe7-C9	1.960	1.984
Fe7-C10	1.924	1.975
Fe7-C11	1.974	1.975
Fe7-C12	1.973	1.976
C8-N13	1.170	1.175
C9-N14	1.17O	1.175
C10-N15	1.170	1.174
C11-N16	1.170	1.175
C12-N17	1.170	1.175

A comparison of tetrazine and tz-mnc(-2) bond lengths show that N1-N2 , N4-N5, N1-C6 lengthen while N2-C3, C3-N4, N5-C6 contract. N1 to N4 distance increases by 0.013 Å.

A comparison of tetrazine and tz-mnc(-3) bond lengths show that N1-N2 , N4-N5, N1-C6, C3-N4 lengthens while N2-C3, N5-C6 contract. N1 to N4 distance has a net elongation of 0.069 Å.

Comparison of tz-mnc(-2) and tz-mnc(-3):

- Fe7-N1 bond is shorter for tz-mnc(-3)
- Fe-CN bonds are longer for tz-mnc(-3)
- C-N bonds are longer for tz-mnc(-3)
- The N1 to N4 lengthening is larger for tz-mnc(-3)
- Effects are larger in quantity for tz-mnc(-3)

Complex tz-mnc(-2) has beta HOMO (Figure 3.6) with π character over the Fe-N bond. It looks like a combination of the LUMO of the tetrazine (with π* character over the N-N bonds and π character over the C-N bond) and a d_{xz} orbital of Fe. The aHOMO (SOMO) (Figure 3.6) is concentrated over the metal fragment.

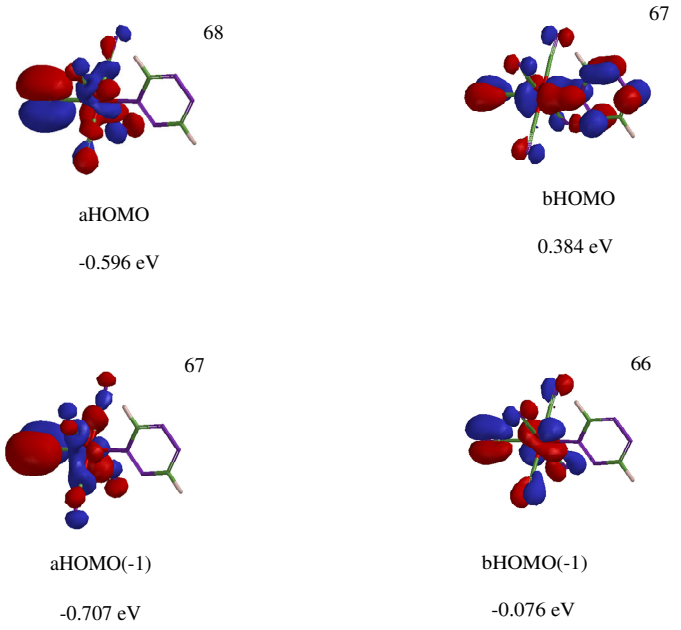

Figure 3.6. HOMO and HOMO(-1) of tz-mnc(-2) complex

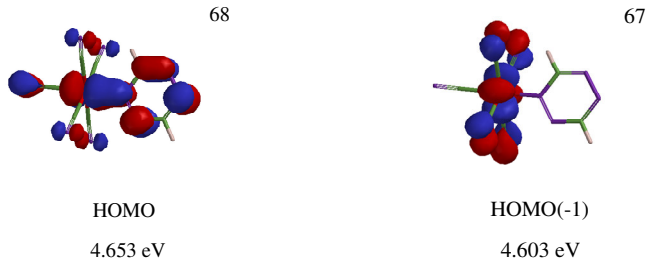

Figure 3.7. HOMO and HOMO(-1) of tz-mnc(-3) complex

Complex tz-mnc(-3) has HOMO with π character over the Fe-N bonds. It looks like a combination of the LUMO of the tetrazine (with π* character over the N-N bonds and π character over the C-N bond) and a d_{xz} orbital of Fe.

Upon one electron reduction of tz-mnc(-2) to tz-mnc(-3), the electron goes to the metal frame and through the Fe-N π bond to tetrazine ring. The tetrazine ring undergoes structural charges indicating gain of electron.

Since the total charges of the two mnc complexes are different, one can not compare the charges on the ligands of the two complexes but charge percentages may give an indication to weather some charge is transferred from metal to ligand. For tz-mnc(-3) (Figure 3.8) the iron atom is less positive; the metal fragment (metal and co-ligands) is more negative, the charge percentage on ligand is higher (18.67%) compared to that of tz-mnc(-2) (9.65%). In Figure 3.8, the circles indicate the fragment on which the charges are added up. The sums are written under the circles. This notation has been adopted for all figures in which charges are displayed throughout this work.

Figure 3.8. Mulliken charges of tz-mnc(-2) and tz-mnc(-3) complexes

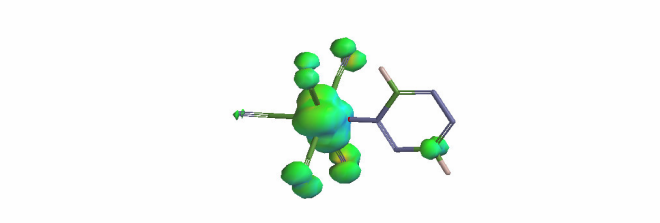

Figure 3.9. Spin of tz-mnc(-2) complex

The spin (Figure 3.9) is observed to be mainly on the metal fragment for the complex with some spin on one of the tetrazine's carbon. This indicates the presence of some metal ligand charge transfer.

3.3.2. DI NUCLEAR COMPLEXES OF TETRAZINE

After a comparison of the behavior of mononuclear complexes, the dinuclear complexes $(\mu\text{-tz-}[Fe(CN)_5]_2)^{4-,\,5-}$, tz-dnc(-4) and tz-dnc(-5), were optimized. The optimized structure and the numbering system are shown in Figure 3.10. The bond lengths are presented in Table 3.4 and Table 3.5.

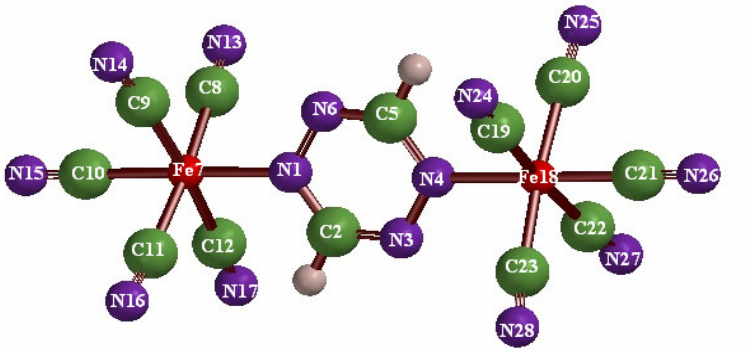

Figure 3.10. Structure and numbering of tetrazine dinuclear complexes

Comparison of tz-mnc(-2) to tz-dnc(-4):

N1-N2, N4-N5 and N1-C6 bonds lengthen, N2-C3, N5-C6 and C3-N4 bonds in tz-mnc(-2) shorten. Fe7-N1 and Fe18-N4 bonds shorten, Fe7-C8, Fe7-C9, Fe7-C11 and Fe7-C12 bonds shorten but Fe7-C10 (same plane with the ring) bond lengthens. C-N bonds lengthen. N1 to N4 distance increases by 0.022 Å. The geometrical behavior of the complex is that of electron enrichment both over the ligand and the metal fragments. The

charge on Fe atoms are the same on tz-mnc(-2) (Figure 3.8) and tz-dnc(-4) (Figure 3.13), the metal frames are more negative while the ligand is slightly less negative.

Table 3.5. Bond lenghts (Å) for tz-dnc(-4) and tz-dnc(-5)complexes

BOND	tz-dnc(-4)	tz-dnc(-5)
N1-N2	1.356	1.378
N1-C6	1.371	1.360
N2-C3	1.312	1.318
N5-C6	1.312	1.318
C3-N4	1.371	1.360
N4-N5	1.356	1.377
N1-N4	2.770	2.800
N1-Fe7	1.919	2.051
Fe7-C8	1.952	1.983
Fe7-C9	1.954	1.982
Fe7-C10	1.950	1.977
Fe7-C11	1.965	1.987
Fe7-C12	1.963	1.987
C8-N13	1.172	1.174
C9-N14	1.172	1.174
C10-N15	1.172	1.174
C11-N16	1.172	1.174
C12-N17	1.172	1.174
N4-Fe18	1.919	2.050
Fe18-C19	1.965	1.988
Fe18-C20	1.963	1.987
Fe18-C21	1.950	1.977
Fe18-C22	1.952	1.983
Fe18-C23	1.954	1.982
C19-N24	1.172	1.174
C20-N25	1.172	1.174
C21-N26	1.172	1.174
C22-N27	1.172	1.174
C23-N28	1.172	1.174

Comparison of tz-dnc(-4) to tz-dnc(-5):

N1-N2, N4-N5, N2-C3, C6-N5 bonds lengthen, N1-C6 and N4-C3 bonds shorten. Fe7-N1 and Fe18-N4 bonds lengthen, Fe-CN bonds lengthen, C-N bonds lengthen. N1 to N4 distance increases by 0.03 Å.

The HOMO of tz-dnc(-4) (Figure 3.11) and the bHOMO of tz-dnc(-5) (Figure 3.12) are alike with π character over the Fe-N bonds. It looks like a combination of the LUMO of the tetrazine (Figure 3.3) (with π* character over the N-N bonds and π character over the C-N bonds) and a d orbital of Fe. The alpha HOMO of tz-dnc(-5) is on the metal frame, indicating the reducing electron is mainly localized on the metal frame.

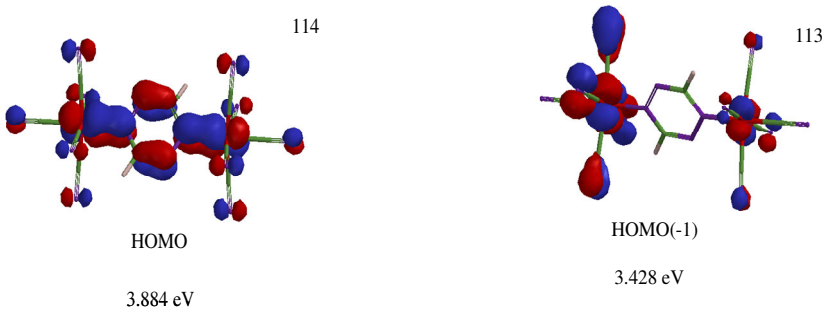

Figure 3.11. HOMO and HOMO(-1) of tz-dnc(-4) complex

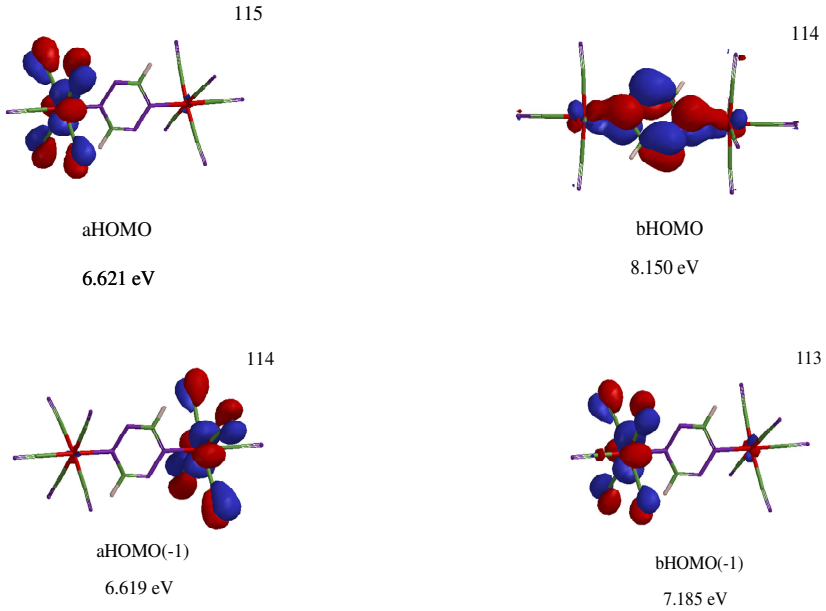

Figure 3.12. HOMO and HOMO(-1) of tz-dnc(-5) complex

For the tz-dnc(-4) and tz-dnc(-5) complexes, charges are distributed equally on the Fe metals. For tz-dnc(-5) (Figure 3.13) the iron atom is less positive. When the tz-dnc(-4) complex takes one electron, bridge ligand tetrazine becomes more negative in tz-dnc(-5) complex. The charge percentage is 4.5 for tz-dnc(-4) and 8.5 for tz-dnc(-5), displaying some electron delocalization to the ligand.

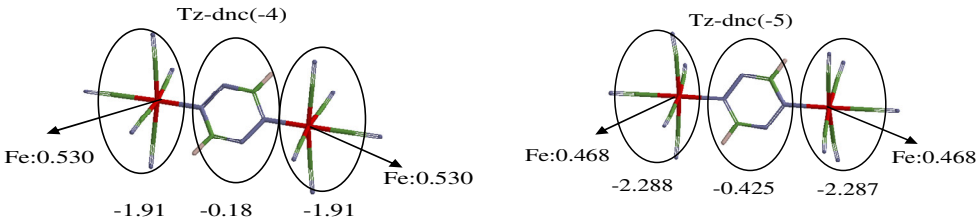

Figure 3.13. Mulliken charges of tz-dnc(-4) and tz-dnc(-5) complexes

The spin on tz-dnc(-5) is observed to be mainly on the metal fragment for the complex with some spin on the carbon of the tetrazine ligand (Figure 3.14). There is more spin on the tetrazine ligand compared to the mononuclear complex.

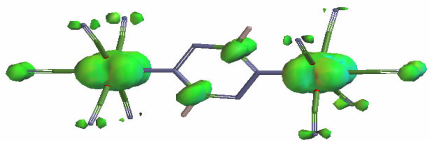

Figure 3.14. Spin of tz-dnc(-5) complex

When the spin, changes in geometrical parameters, and charges are considered, more metal to ligand charge transfer (MLCT) seem to occur in the tz-dnc(-5).

3.3.3. TRI NUCLEAR COMPLEXES OF TETRAZINE

The geometrical structure and electronic distribution of the mixed valent trinuclear complexes of $[Fe(CN)_5\text{-}\mu\text{-}L\text{-}Fe(CN)_4\text{-}L\text{-}Fe(CN)_5]^{n-}$, n = 5, 6, 7; L= tz are introduced here.

The optimized structure and the numbering system is shown in Figure 3.15. The bond lengths are present in Table 3.6.

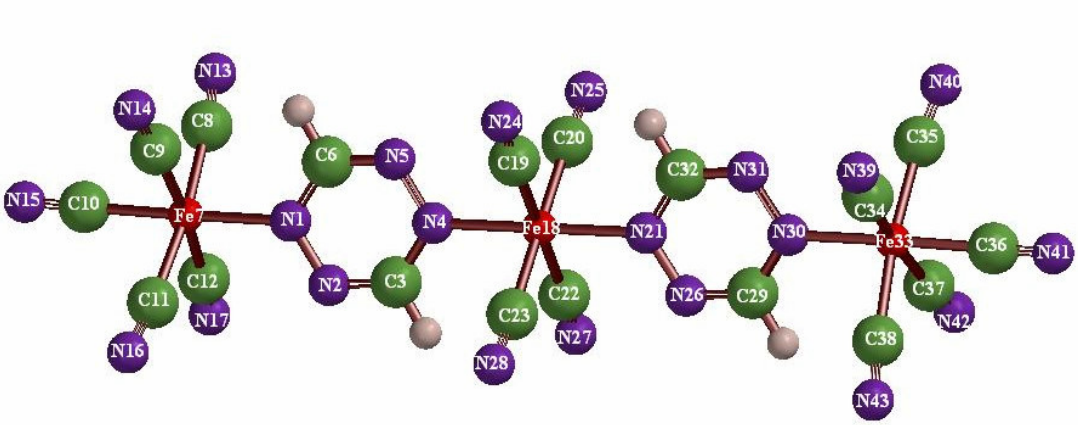

Figure 3.15. Structure and numbering of tetrazine trinuclear trans complex

We have modeled the cis isomers of the complexes as well as shown in Figure 3.16. The trans isomers are lower in energy than cis isomers. The numbering system for cis and trans isomers are identical.

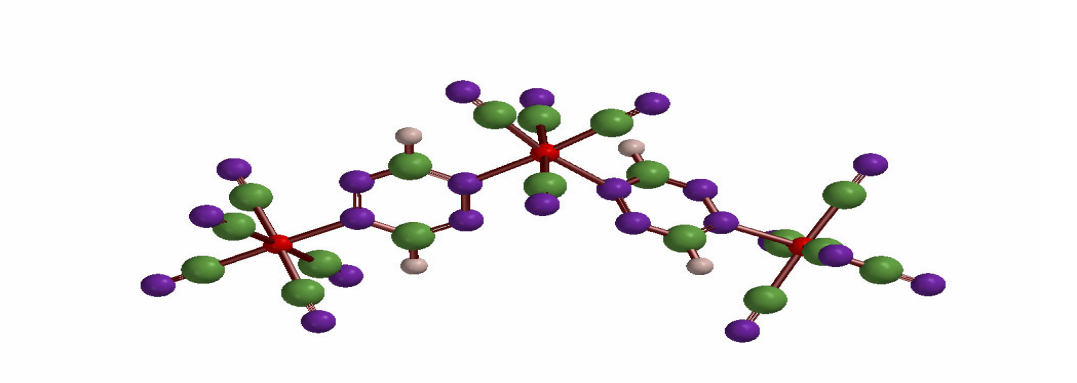

Figure 3.16. Structure of tetrazine trinuclear cis complex

Table 3.6. Bond lenghts (Å) for tz-tnc complexes

BOND	tz-tnc(-5) trans	tz-tnc(-5) cis	tz-tnc(-6) trans	tz-tnc(-6) cis	tz-tnc(-7) trans	tz-tnc(-7) cis
N1-N2	1.326	1.327	1.347	1.349	1.380	1.380
N1-C6	1.355	1.359	1.364	1.368	1.363	1.363
N2-C3	1.334	1.333	1.323	1.321	1.322	1.322
N5-C6	1.328	1.329	1.321	1.321	1.318	1.319
C3-N4	1.346	1.344	1.360	1.362	1.358	1.359
N4-N5	1.327	1.332	1.343	1.349	1.381	1.381
N1-N4	2.736	2.740	2.774	2.782	2.805	2.813
N1-Fe7	2.048	2.024	1.984	1.968	2.057	2.059
Fe7-C8	1.978	1.974	1.973	1.973	1.993	1.988
Fe7-C9	1.978	1.972	1.972	1.970	1.992	1.992
Fe7-C10	1.930	1.932	1.951	1.955	1.988	1.988
Fe7-C11	1.967	1.967	1.962	1.964	1.987	1.989
Fe7-C12	1.966	1.968	1.967	1.968	1.988	1.988
C8-N13	1.171	1.170	1.173	1.173	1.174	1.174
C9-N14	1.171	1.170	1.173	1.173	1.174	1.174
C10-N15	1.171	1.171	1.174	1.174	1.175	1.175
C11-N16	1.171	1.171	1.173	1.173	1.174	1.174
C12-N17	1.171	1.171	1.173	1.173	1.174	1.174
N4-Fe18	2.044	2.153	1.992	2.046	2.098	2.202
Fe18-C19	1.969	1.913	1.971	1.927	1.986	1.940
Fe18-C20	1.966	1.913	1.971	1.925	1.986	1.940
Fe18-N21	2.043	2.158	1.990	2.055	2.100	2.216
Fe18-C22	1.967	1.957	1.970	1.959	1.986	1.970
Fe18-C23	1.968	1.974	1.972	1.977	1.987	1.984
C19-N24	1.170	1.171	1.172	1.172	1.172	1.172
C20-N25	1.170	1.170	1.172	1.171	1.172	1.172
C22-N27	1.170	1.170	1.172	1.171	1.172	1.172
C23-N28	1.170	1.171	1.172	1.173	1.172	1.174
N21-N26	1.328	1.332	1.343	1.352	1.375	1.383
N26-C29	1.329	1.328	1.321	1.317	1.318	1.317
C29-N30	1.355	1.358	1.364	1.368	1.363	1.363
N30-N31	1.327	1.325	1.347	1.348	1.380	1.380
N31-C32	1.333	1.335	1.323	1.324	1.322	1.324
C32-N21	1.346	1.345	1.361	1.360	1.358	1.357
N21-N30	2.737	2.743	2.774	2.787	2.806	2.817
N30-Fe33	2.048	2.040	1.981	1.968	2.061	2.057
Fe33-C34	1.967	1.966	1.963	1.967	1.988	1.992
Fe33-C35	1.966	1.967	1.966	1.976	1.987	1.994
Fe33-C36	1.930	1.931	1.952	1.955	1.988	1.989
Fe33-C37	1.978	1.977	1.974	1.971	1.992	1.988
Fe33-C38	1.977	1.976	1.971	1.962	1.992	1.986
C34-N39	1.171	1.171	1.173	1.173	1.174	1.174
C35-N40	1.171	1.171	1.173	1.173	1.174	1.174
C36-N41	1.171	1.171	1.174	1.174	1.175	1.175
C37-N42	1.171	1.171	1.173	1.173	1.174	1.174
C38-N43	1.171	1.171	1.173	1.173	1.174	1.174

N to N distances for the ligand increases with reduction and are even longer for cis isomers. Fe-C bond lengths of tz-tnc(-5) decrease for tz-tnc(-6) and increase for tz-tnc(-7) (to longer lengths than those of tz-tnc(-5)) on terminal metal fragments but on the middle metal fragment, comparison of tz-tnc(-5) to tz-tnc(-6) shows a slightly increase. C-N bond lengths increase slightly with reduction and cis, trans isomers do not differ in C-N bond lengths.

For both cis and trans isomers Fe-N bond lengths of tz-tnc(-5) are observed to decrease for tz-tnc(-6) and increase for tz-tnc(-7) (to longer lengths than tz-tnc(-5). Fe-N bonds are longer around the middle metal fragment.

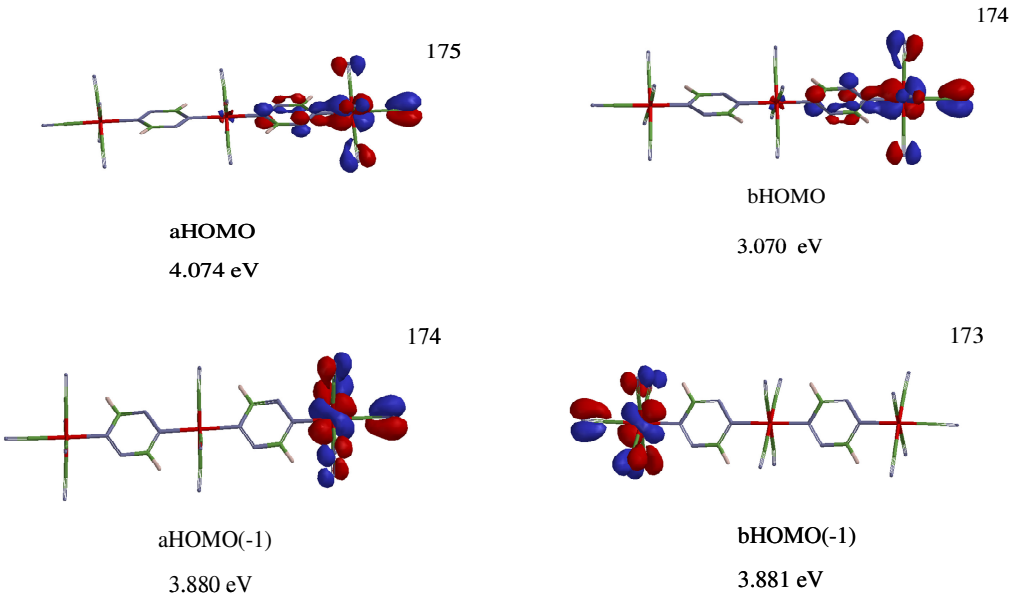

Figure 3.17. HOMO and HOMO(-1) of tz-tnc(-5)trans complex

The molecular orbital diagram alpha HOMO and beta HOMO for tz-tnc(-5) (Figure 3.17, 3.18) each show a π bond on Fe-N on one terminal metal fragment.

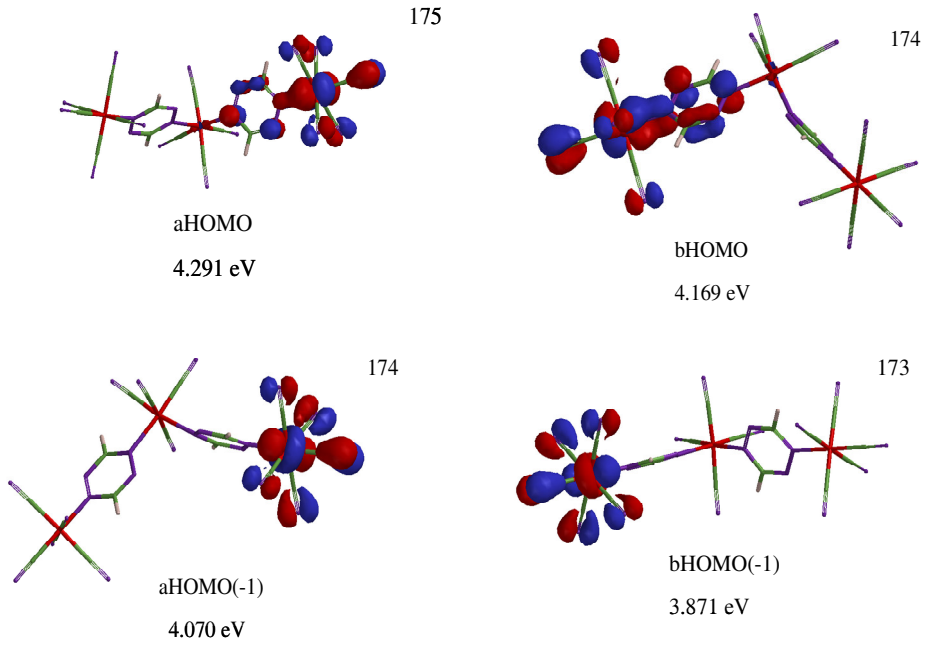

Figure 3.18. HOMO and HOMO(-1) of tz-tnc(-5)cis complex

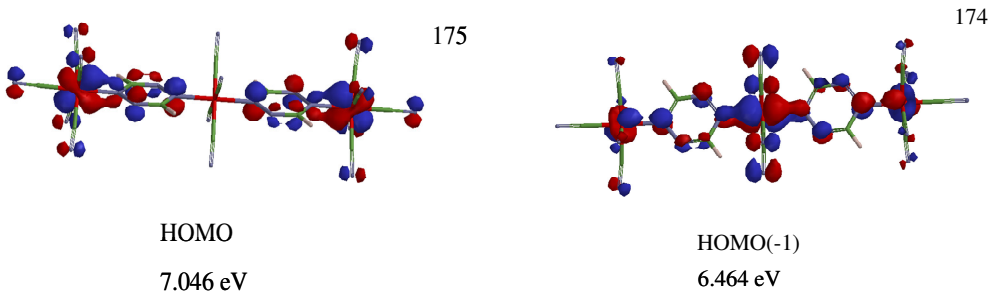

Figure 3.19. HOMO and HOMO(-1) of tz-tnc(-6)trans complex

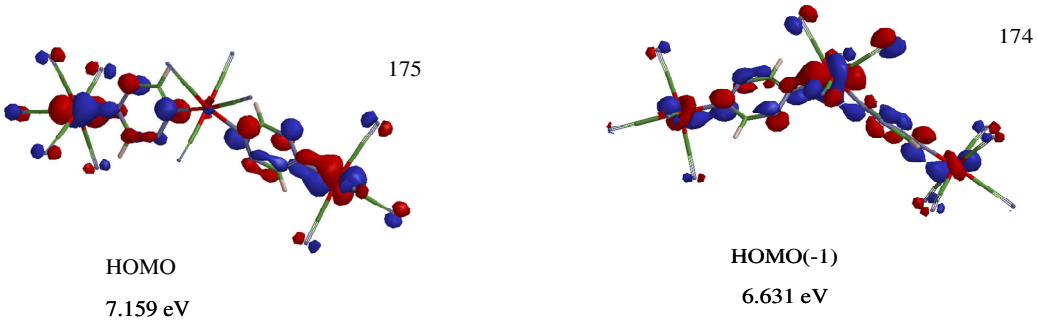

Figure 3.20. HOMO and HOMO(-1) of tz-tnc(-6)cis complex

Tz-tnc(-6) (Figure 3.19, 3.20) molecular orbital diagram for HOMO show π on Fe-N bonds on both terminus and π for all Fe-N bonds in HOMO(-1). HOMO(-1) has stronger π overlaps fort he central metal fragment. Hence the shortening of Fe-N bonds is explained.

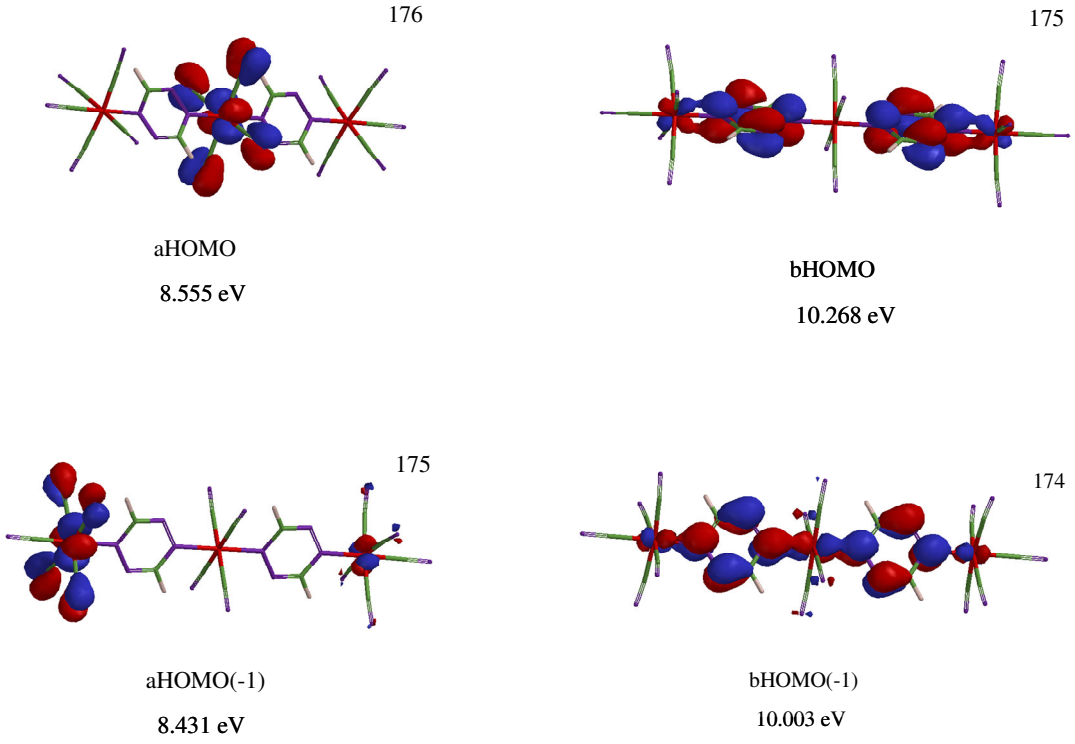

Figure 3.21. HOMO and HOMO(-1) of tz-tnc(-7)trans complex

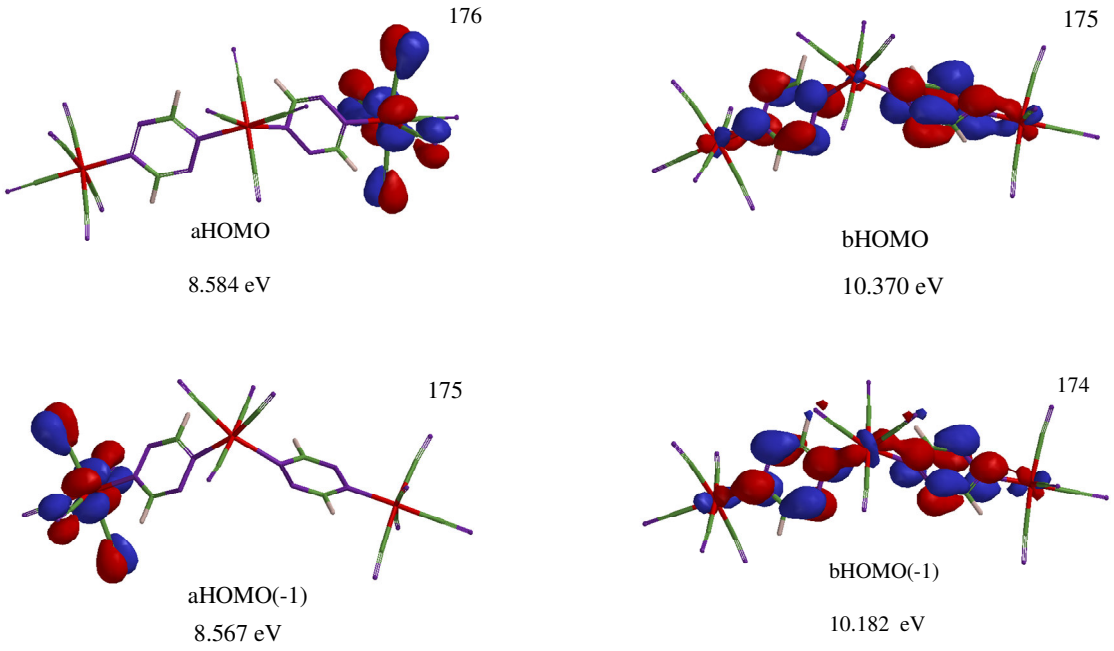

Figure 3.22. HOMO and HOMO(-1) of tz-tnc(-7)cis complex

Tz-tnc(-7) (Figure 3.21, 3.22) has alpha HOMO concentrated on middle metal fragment, beta HOMO showing π bond on Fe-N terminal fragments and beta HOMO(-1) with π bond on all Fe-N bonds. Similar diagram are observed for the cis isomers as well.

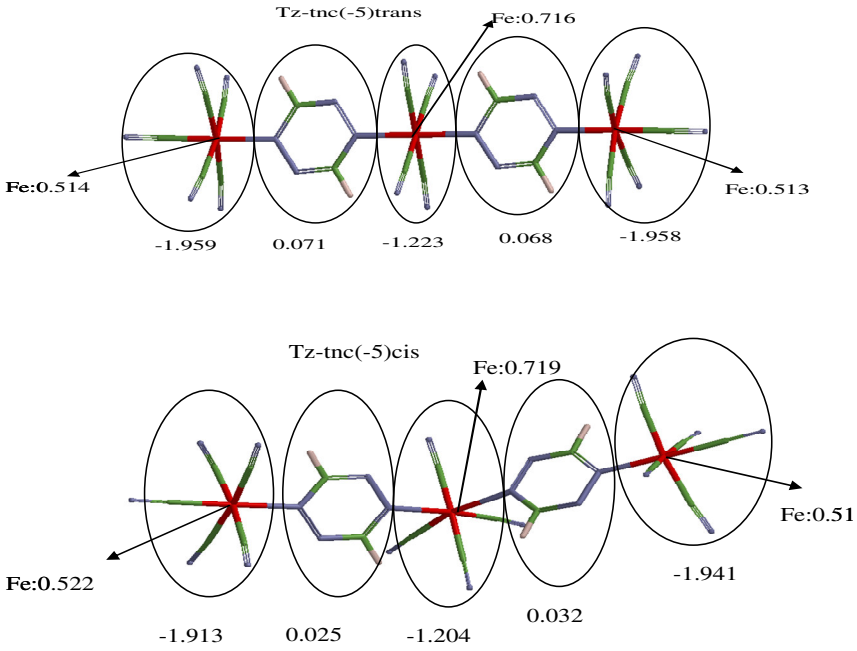

Figure 3.23. Mulliken charges of tz-tnc(-5)trans and tz-tnc(-5)cis complexes

The mulliken charge distribution are shown in Figure 3.23. The tetrazine ligand is positively charged in tz-tnc(-5) in Figure 3.23.

Reduction increases charge percent on tetrazine ligand to 1.75 in tz-tnc(-6) (cis being higher ~2.7 %) in Figure 3.24.

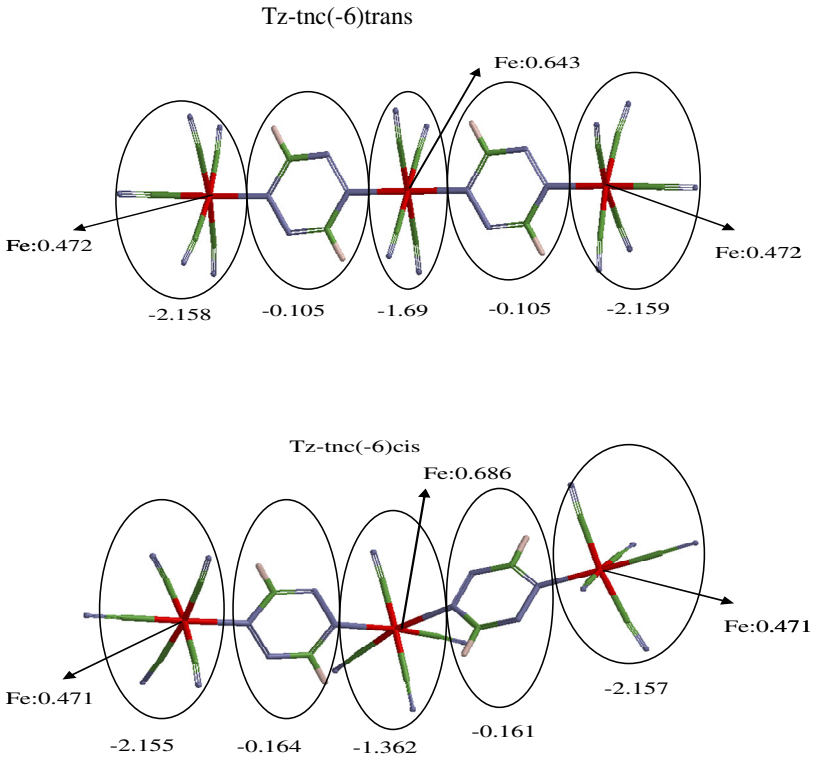

Figure 3.24. Mulliken charges of tz-tnc(-6)trans and tz-tnc(-6)cis complexes

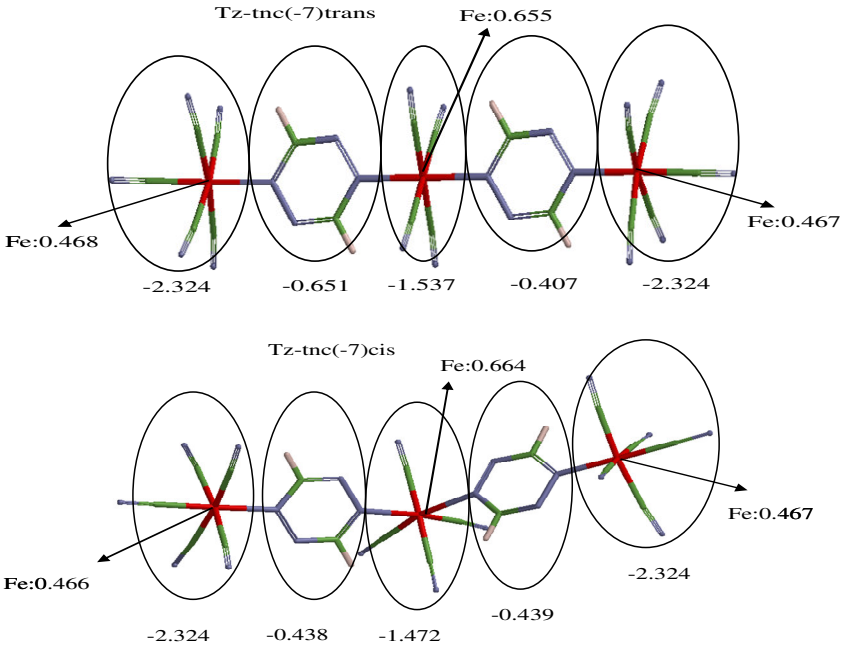

Figure 3.25. Mulliken charges of tz-tnc(-7)trans and tz-tnc(-7)cis complexes

Reduction to tz-tnc(-7) (Figure 3.25) increases charge percentage on tetrazine to 6-9 %.

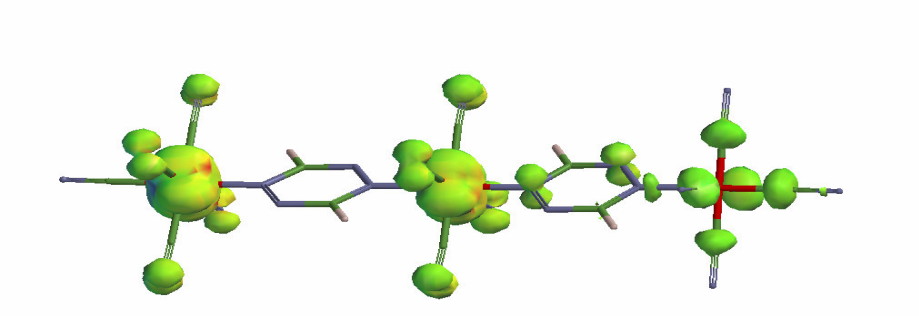

Figure 3.26. Spin of tz-tnc(-5)trans complex

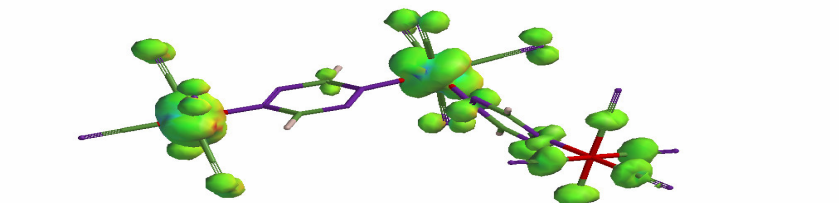

Figure 3.27. Spin of tz-tnc(-5)cis complex

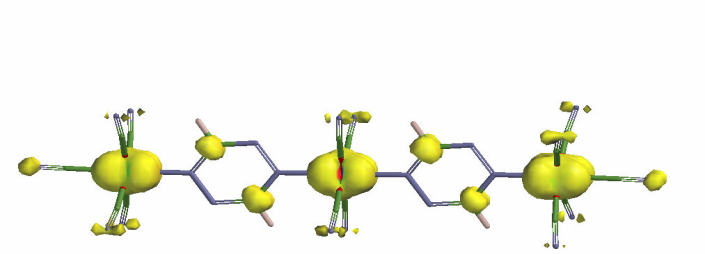

Figure 3.28. Spin of tz-tnc(-7)trans complex

The spin is observed to be mainly on the metal fragment for the complex with some spin on tetrazine's carbons. The spin distribution on the ligands seem to be different for cis and trans isomers. The spin on tetrazine for the tz-tnc(-5)trans complex (Figure 3.26) is on one ring only while the spin is observed on both tetrazine rings for the tz-tnc(-5)cis complex (Figure 3.27), spin is on both rings for both trans and cis tz-tnc(-7) complex (Figure 3.28, 3.29). As reduction proceeds, metal to ligand charge transfer proceeds too.

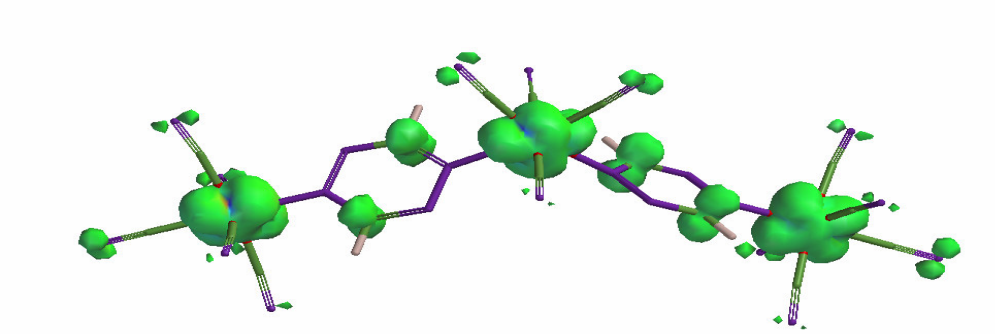

Figure 3.29. Spin of tz-tnc(-7)cis complex

When the charge percentages on the ligand of mnc(-2) and dnc(-4) compound it is observed that the charge percentages for dnc complex are about half of those in the mnc complex. This is also true for this reduced forms of tz-mnc(-3) and tz-dnc(-5).

For tnc, the situation is different. The metal fragment in the center having four CN coligand and bound to two tetrazines is more electronegative than the tetrazine metal fragments. It seems that the terminal metal fragments are back bonding through the Fe-N π Bonds but the central metal frame doesn't. Bond lengths of central Fe-N bonds are longer than tetrazine Fe-N bonds. Reduction of tz-tnc(-5) to tz-tnc(-6) shows contraction of all Fe-N bonds which may be due to more back bonding and the charge distribution also is indicative of this kind of behavior.

3.4. PYRAZINE COMPLEXES

The approach taken for tetrazine is similarly taken for pyrazine. The mononuclear $[pyz\text{-}Fe(CN)_5]^{2-,3-}$ complexes were optimized (Figure 3.30). The bond lengths are presented in Table 3.7.

3.4.1. MONO NUCLEAR PYRAZINE COMPLEXES

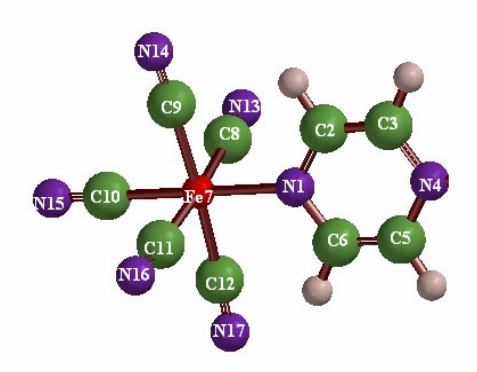

Figure 3.30. Structure and numbering of pyrazine mononuclear complex

Table 3.7. Bond lengths (Å) pyz-mnc(-2) and pyz-mnc(-3)complexes

BOND	pyz-mnc(-2)	pyz-mnc(-3)
N1-C2	1.343	1.365
N1-C6	1.343	1.365
C2-C3	1.393	1.384
C5-C6	1.392	1.384
N4-C3	1.339	1.352
N4-C5	1.340	1.352
N1-N4	2.818	2.885
N1-Fe7	2.072	1.943
Fe7-C8	1.971	1.982
Fe7-C9	1.970	1.982
Fe7-C10	1.917	1.965
Fe7-C11	1.971	1.982
Fe7-C12	1.972	1.982
C8-N13	1.172	1.177
C9-N14	1.172	1.177
C10-N15	1.171	1.176
C11-N16	1.172	1.177
C12-N17	1.172	1.177

A comparison of pyrazine and pyz-mnc(-2) bond lengths show slight changes. N1-C2, C3-N4, N4-N5 and N1-C6 bonds lengthen while C2-C3 and C5-C6 bonds shorten slightly. N1-C6 lengtening, N4-N5 lengthening and C5-C6 bonds shortening is equal to N1-C2 and C3-N4 bond lengthening and C2-C3 bond shortening. N1 to N4 distance increases by only 0.001 Å, remaining almost the same.

A comparison of pyz and pyz-mnc(-3) bond lengths show that N1-C2 , C3-N4, N4-C5 and N1-C6 bonds lengthen while C2-C3 and C5-C6 bonds shorten. N1-C6 and N4-C5 bonds lengthening and C5-C6 bond shortening is equal to N1-C2 and C3-N4 bonds lengthening and C2-C3 bond shortening. N1 to N4 distance increases by 0.066 Å.

Comparison of pyz-mnc(-2) and pyz-mnc(-3):

- When pyrazine makes the complex $[pyz\text{-}Fe(CN)_5]^{2-}$ the N1 to N4 distance increases only 0.001 Å but in $[pyz\text{-}Fe(CN)_5]^{3-}$ complex, N1 to N4 distance increases 0.066 Å.
- Fe7-N1 bond is shorter for pyz-mnc(-3) complex.
- Fe-CN bonds are longer for pyz-mnc(-3)
- C-N bonds are longer for pyz-mnc(-3) complex.

Pyz-mnc(-2) complex has alpha HOMO and beta HOMO (Figure 3.31) concentrated over the metal fragment. Pyrazine mononuclear complex, pyz-mnc(-2) does not show a π bond over Fe-N bond. Pyz-mnc(-3) have the same HOMO character as that of tetrazine analogue. Pyz-mnc(-3) has HOMO (Figure 3.32) with π character over the Fe-N bonds. This MO is (π bond) an overlap of d orbital of iron and LUMO of pyrazine (Figure 3.4). Upon one electron reduction, the electron goes to metal frame and through the π bond over Fe-N the bond to pyrazine ligand strengthens.

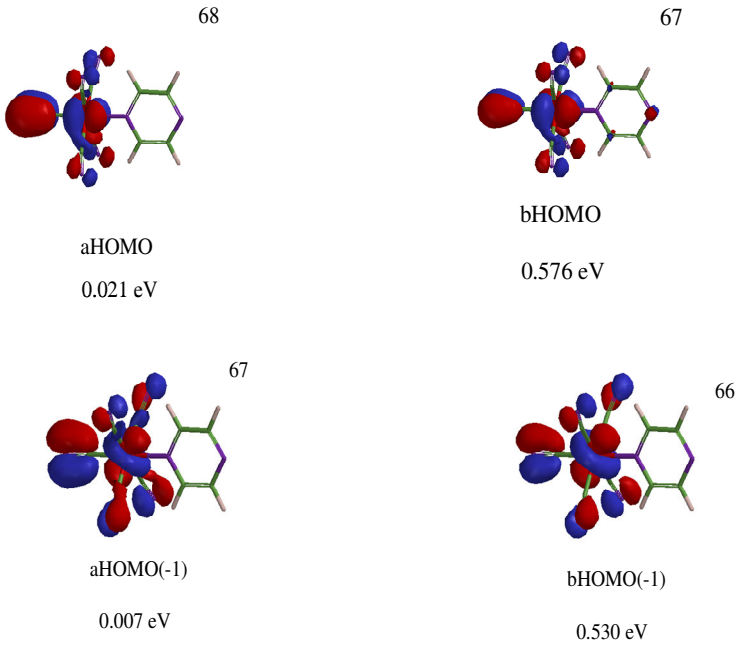

Figure 3.31. HOMO and HOMO(-1) of pyz-mnc(-2) complex

Figure 3.32. HOMO and HOMO(-1) of pyz-mnc(-3) complex

Pyz-mnc(-2) has positive charge on pyrazine ligand; charge percentage for pyz-mnc(-3) is 11.73%. Some metal ligand charge transfer has occurred. Although the metal frame gets the electron, some donation to the ligand is taking place through the Fe-N π bond in pyz-mnc(-3) (Figure 3.33).

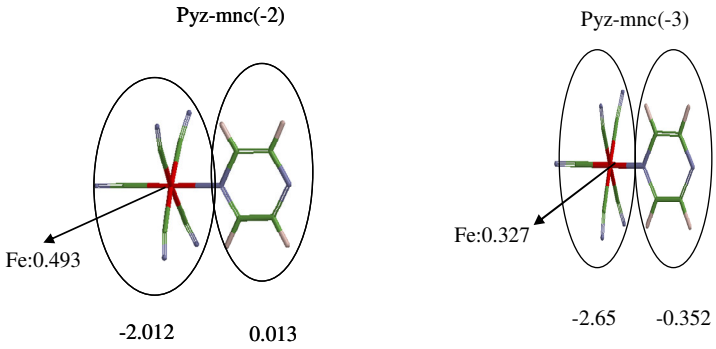

Figure 3.33. Mulliken charges of pyz-mnc(-2) and pyz-mnc(-3) complexes

The spin (Figure 3.34) is observed to be mainly on the metal fragment for the complex pyz-mnc(-2). No spin is observed on the ligand pyrazine.

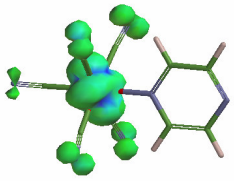

Figure 3.34. Spin of pyz-mnc(-2) complex

3.4.2. DI NUCLEAR COMPLEXES OF PYRAZINE

After comparing the behavior of mono nuclear complexes, the dinuclear complexes pyz-$[Fe(CN)_5]_2^{4-,\ 5-}$ were optimized. The optimized structure and the numbering system is shown in Figure 3.35. The bond lengths are presented in Table 3. 8.

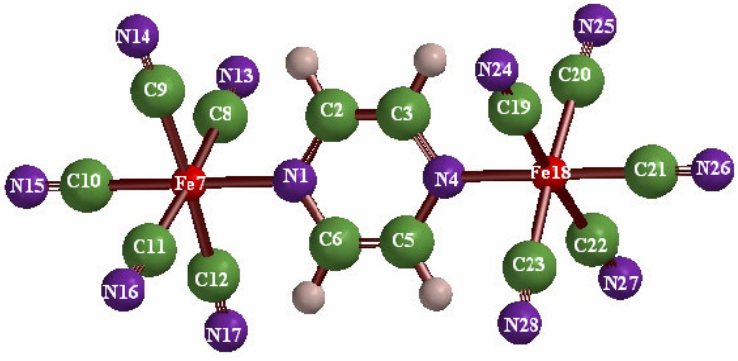

Figure 3.35. Structure and numbering of pyrazine dinuclear complex

Table 3.8. Bond lenghts (Å) for pyz-dnc(-4) and pyz-dnc(-5)complexes

BOND	pyz-dnc(-4)	pyz-dnc(-5)
N1-C2	1.353	1.369
N1-C6	1.353	1.369
C2-C3	1.387	1.381
C5-C6	1.387	1.381
N4-C3	1.353	1.369
N4-C5	1.353	1.369
N1-N4	2.843	2.908
N1-Fe7	2.041	2.044
Fe7-C8	1.960	1.984
Fe7-C9	1.954	1.982
Fe7-C10	1.924	1.971
Fe7-C11	1.953	1.984
Fe7-C12	1.963	1.982
C8-N13	1.173	1.175
C9-N14	1.173	1.175
C10-N15	1.173	1.175
C11-N16	1.173	1.175
C12-N17	1.173	1.175
N4-Fe18	2.041	2.043
Fe18-C19	1.963	1.984
Fe18-C20	1.963	1.982
Fe18-C21	1.924	1.971
Fe18-C22	1.954	1.984
Fe18-C23	1.960	1.982
C19-N24	1.173	1.175
C20-N25	1.173	1.175
C21-N26	1.173	1.175
C22-N27	1.173	1.175
C23-N28	1.173	1.175

Comparison of pyz-mnc(-2) and pyz-dnc(-4):

N1-C2, N1-C6, N4-C3 and N4-C5 bonds lengthen and C2-C3 and C5-C6 bonds shorten. Fe7-N1 bond is longer for pyz-mnc(-2). Fe7-C8, Fe7-C9, Fe7-C11 and Fe7-C12 bonds are longer for pyz-mnc(-2) and Fe7-C10 is longer for pyz-dnc(-4). C-N bonds are longer for pyz-dnc(-4). N1 to N4 distance increases by 0.025 Å.

Charges on the Fe atoms on pyz-mnc(-2) and pyz-dnc(-4) are almost the same. Ligand pyrazine is much more positive in pyz-dnc(-4).

Comparison of pyz-dnc(-4) and pyz-dnc(-5):

N1-C2, C3-N4, N1-C6 and N4-C5 bonds lengthen and C2-C3 and C5-C6 bonds shorten. Fe7-N1 and Fe18-N4 bonds are very slightly longer for pyz-dnc(-5), Fe-CN and C-N bonds are longer for pyz-dnc(-5). N1 to N4 distance increases by 0.065 Å for pyz-dnc(-5).

HOMO of pyz-dnc(-4)(index 114) (Figure 3.36) has some π character for Fe-N which looks like LUMO of pyrazine (Figure 3.4) overlapping with d of Fe.

For pyz-dnc(-5) the same picture is observed for beta HOMO (index 114) (Figure 3.37) with SOMO (index 115) being completely on metal fragment.

Dinuclear complexes of pyz and tz have the same characters for their HOMOs. Again the geometrical changes in the complexes are well explained by the frontier orbitals' characters.

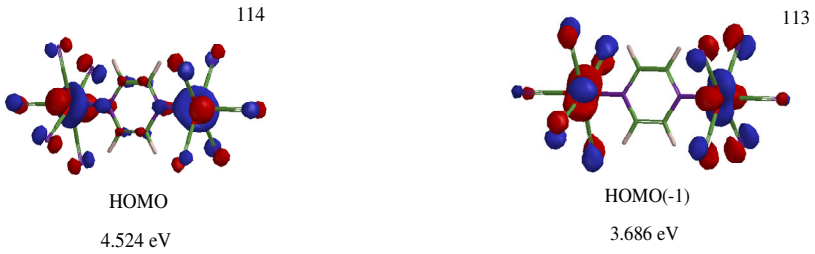

Figure 3.36. HOMO and HOMO(-1) of pyz-dnc(-4) complex

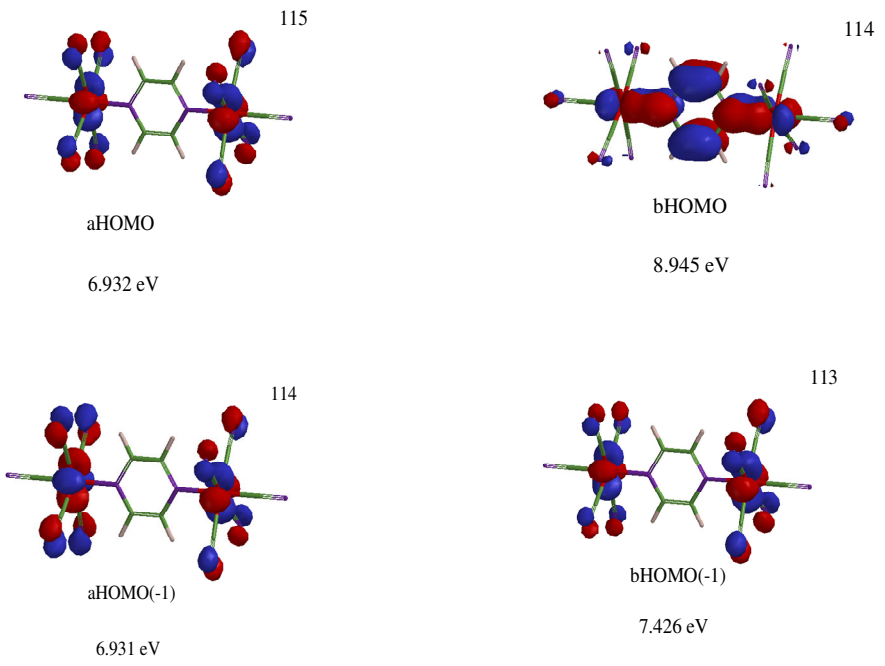

Figure 3.37. HOMO and HOMO(-1) of pyz-dnc(-5) complex

Charges are distributed equally on Fe metals both of pyz-dnc(-4) and pyz-dnc(-5) complexes (Figure 3.38). When the pyz-dnc(-4) complex gains one electron, the metal frames become more negative and pyrazine ligand's Mulliken charge which was positive becomes negative. The charge percentage is 4.34 % on the ligand. The charges on both metals to be equal with some charge on the ligand can be attributed to electron delocalization to some extent.

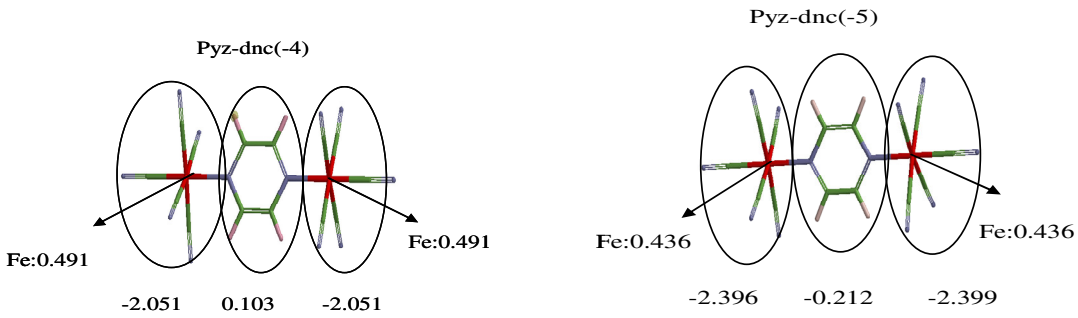

Figure 3.38. Mulliken charges of pyz-dnc(-4) and pyz-dnc(-5) complexes

The spin is observed to be on the metal fragment for the pyz-dnc(-5) complex (Figure 3.39). There is no spin observed on the pyrazine ligand. Similar to charge distribution, the symmetry of spin on both metals may be attributed to the electron to be mainly localized on metal frames with some delocalization on the ligand.

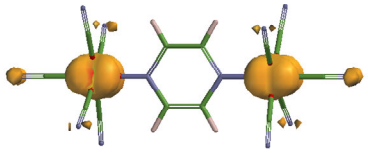

Figure 3.39. Spin of pyz-dnc(-5) complex

3.4.3.TRI NUCLEAR COMPLEXES OF PYRAZINE

The approach taken for trinuclear tetrazine complexes has also been adopted for the trinuclear complexes of pyrazine. The cis and trans isomers were optimized (Figure 3.40 and Figure 3.41). The bond lengths for each complex are presented in Table 3.9. The trans isomers are lower in energy than cis isomers. The numbering system for cis and trans isomers are identical.

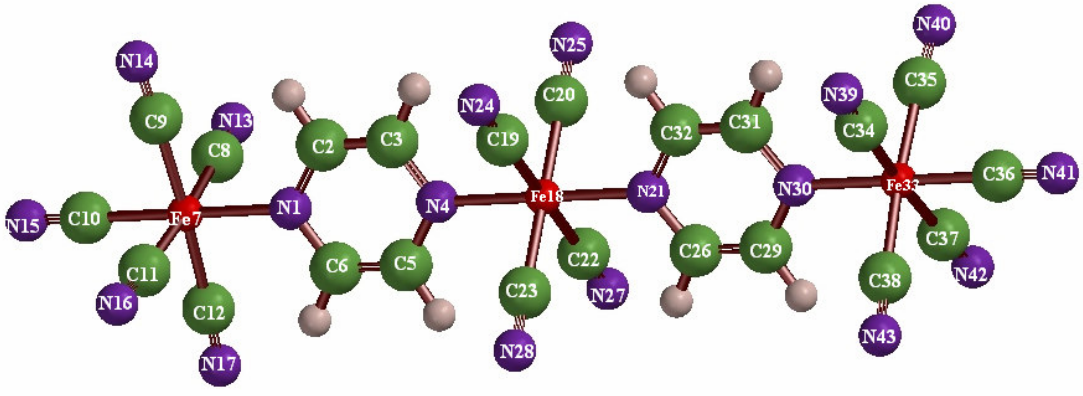

Figure 3.40. Structure and numbering of pyrazine trinuclear trans complex

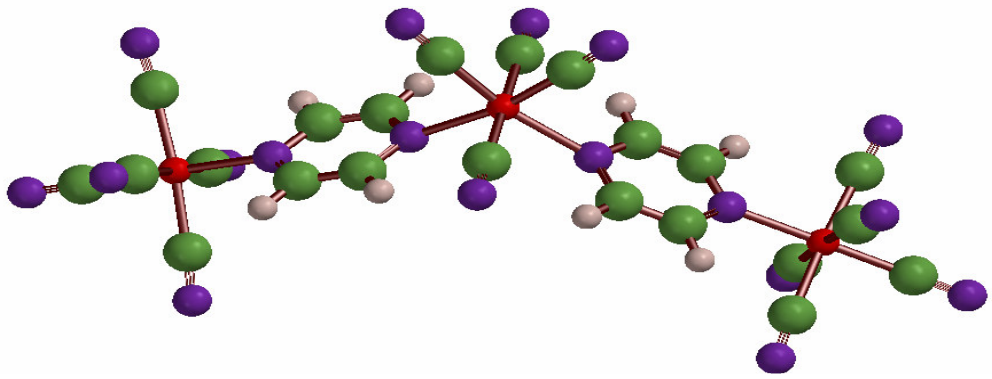

Figure 3.41. Structure of pyrazine trinuclear cis complex

A comparison of cis pyz-tnc(-5,-6,-7) and trans pyz-tnc(-5,-6,-7) bond lengths show that Fe18-C19, Fe18-C20, Fe18-C22 and Fe18-C23 bonds shorten while N4-Fe18 and Fe18-N21 bonds lengthen for pyz-tnc(-5, -6, -7)cis complexes. N1 to N4 and N21 to N30 distance increase about 0.004 Å. In other words the trans and cis isomers differ only around the central metal fragment.

A comparison of trans pyz-tnc(-5), pyz-tnc(-6) and pyz-tnc(-7) bond lengths show that N1 to N4 distances of the ligands increase with reduction and are slightly longer for cis isomers. Fe-C bond lengths of pyz-tnc(-5) increases for pyz-tnc(-6) and increase for pyz-tnc(-7) (to longer lengths than pyz-tnc(-5)). C-N bond lengths increase with reduction Fe-N bond lengths of pyz-tnc(-5) increase for pyz-tnc(-6) and decrease for pyz-tnc(-7) (to smaller lengths than those for pyz-tnc(-5). This trend is the opposite to the observed trend for tz-tnc complexes. The trend for trans pyz-tnc(-5) and pyz-tnc(-6) structures show that Fe-N bonds are shorten for central metal fragment. The trend for cis pyz-tnc complexes and pyz-tnc(-7) is similar to the trend observed for tetrazine tri nuclear complexes.

Table 3.9. Bond lengths (Å) for pyz-tnc complexes

BOND	pyz-tnc(-5) trans	pyz-tnc(-5) cis	pyz-tnc(-6) trans	pyz-tnc(-6) cis	pyz-tnc(-7) trans	pyz-tnc(-7) cis
N1-C2	1.345	1.344	1.368	1.349	1.368	1.365
C2-C3	1.394	1.395	1.397	1.394	1.387	1.388
C3-C4	1.345	1.347	1.348	1.351	1.362	1.365
N4-C5	1.345	1.346	1.348	1.350	1.362	1.365
C5-C6	1.394	1.396	1.397	1.396	1.387	1.388
N1-C6	1.345	1.344	1.346	1.349	1.367	1.366
N1-N4	2.831	2.835	2.854	2.859	2.909	2.913
N1-Fe7	2.179	2.193	2.239	2.157	2.086	2.077
Fe7-C8	1.972	1.972	1.959	1.962	1.988	1.987
Fe7-C9	1.973	1.977	1.958	1.963	1.986	1.985
Fe7-C10	1.921	1.920	1.929	1.928	1.969	1.972
Fe7-C11	1.972	1.968	1.959	1.963	1.988	1.984
Fe7-C12	1.973	1.974	1.958	1.965	1.986	1.988
C8-N13	1.172	1.172	1.175	1.175	1.176	1.176
C9-N14	1.171	1.171	1.176	1.175	1.177	1.176
C10-N15	1.172	1.172	1.175	1.175	1.177	1.177
C11-N16	1.172	1.172	1.175	1.174	1.176	1.176
C12-N17	1.171	1.171	1.176	1.175	1.177	1.176
N4-Fe18	2.075	2.216	2.150	2.208	2.102	2.233
Fe18-C19	1.967	1.916	1.963	1.910	1.982	1.928
Fe18-C20	1.968	1.958	1.961	1.911	1.981	1.929
Fe18-N21	2.078	2.211	2.102	2.262	2.076	2.251
Fe18-C22	1.967	1.916	1.963	1.958	1.982	1.967
Fe18-C23	1.968	1.960	1.961	1.959	1.981	1.967
C19-N24	1.170	1.169	1.175	1.174	1.174	1.174
C20-N25	1.170	1.171	1.174	1.174	1.174	1.174
C22-N27	1.170	1.169	1.175	1.176	1.174	1.176
C23-N28	1.170	1.171	1.174	1.176	1.174	1.176
N21-C26	1.346	1.346	1.347	1.349	1.365	1.364
C26-C29	1.394	1.396	1.397	1.396	1.385	1.389
C29-N30	1.344	1.344	1.346	1.348	1.368	1.365
N30-C31	1.344	1.344	1.346	1.348	1.368	1.366
C31-C32	1.394	1.395	1.397	1.396	1.385	1.388
C32-N21	1.346	1.347	1.347	1.349	1.365	1.364
N21-N30	2.826	2.834	2.851	2.859	2.907	2.914
N30-Fe33	2.136	2.180	2.223	2.203	2.061	2.086
Fe33-C34	1.973	1.969	1.958	1.965	1.987	1.989
Fe33-C35	1.972	1.976	1.960	1.962	1.987	1.985
Fe33-C36	1.925	1.922	1.930	1.925	1.976	1.970
Fe33-C37	1.973	1.972	1.958	1.960	1.987	1.987
Fe33-C38	1.972	1.975	1.960	1.960	1.987	1.985
C34-N39	1.171	1.172	1.176	1.175	1.176	1.176
C35-N40	1.172	1.171	1.175	1.175	1.176	1.176
C36-N41	1.172	1.172	1.175	1.175	1.177	1.177
C37-N42	1.171	1.172	1.176	1.175	1.176	1.176
C38-N43	1.172	1.171	1.175	1.175	1.176	1.176

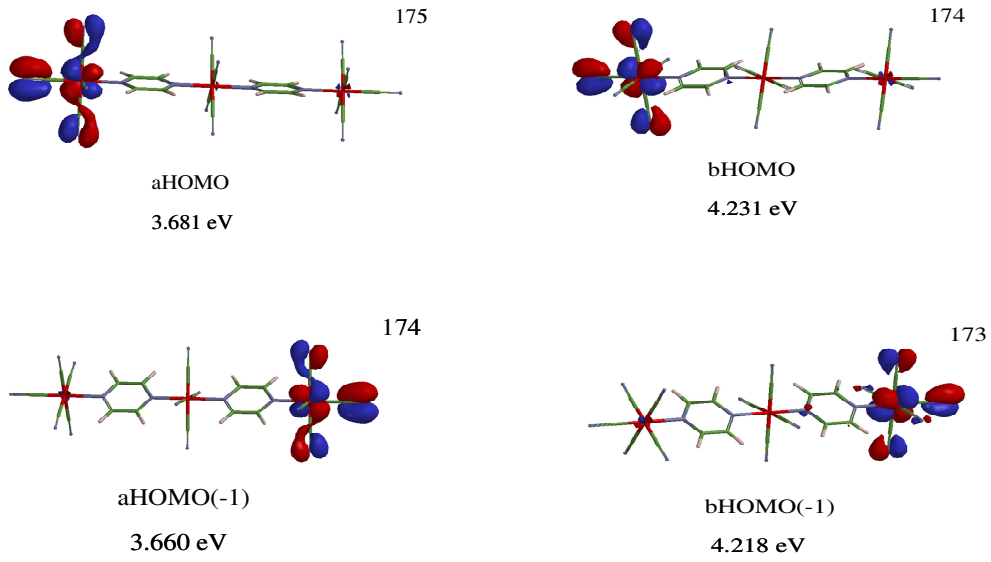

Figure 3.42. HOMO and HOMO(-1) of pyz-tnc(-5)trans complex

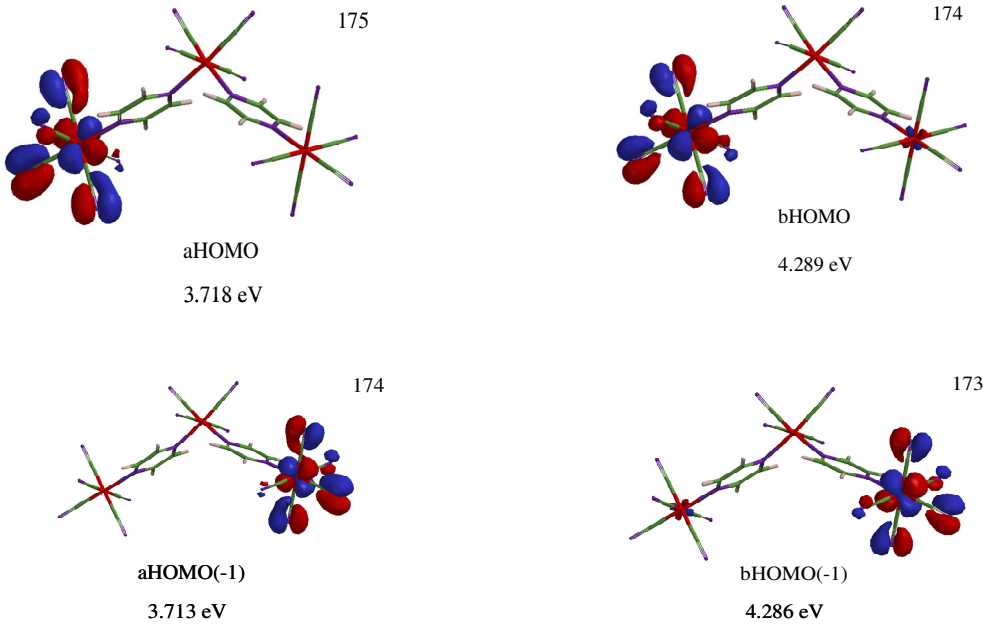

Figure 3.43. HOMO and HOMO(-1) of pyz-tnc(-5)cis complex

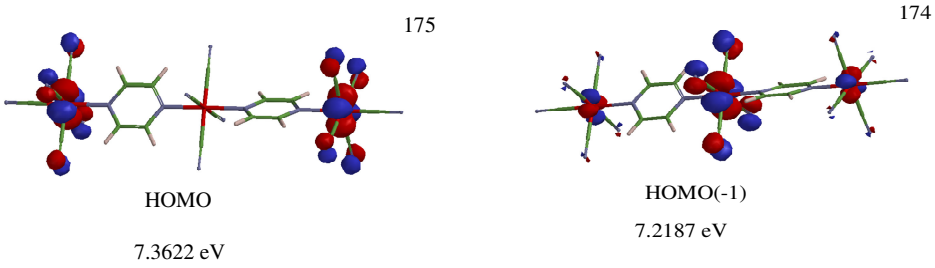

Figure 3.44. HOMO and HOMO(-1) of pyz-tnc(-6)trans complex

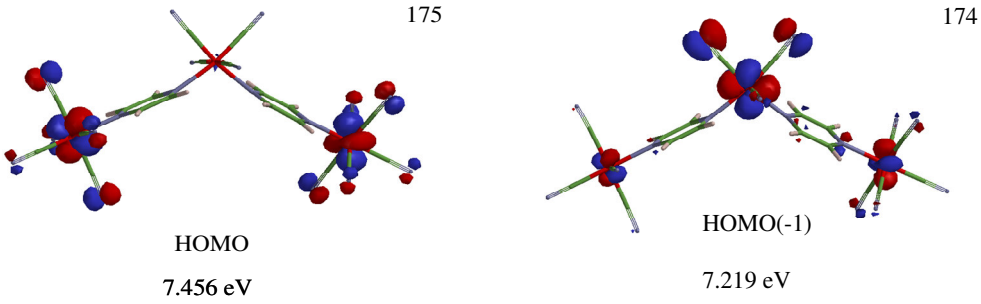

Figure 3.45. HOMO and HOMO(-1) of pyz-tnc(-6)cis complex

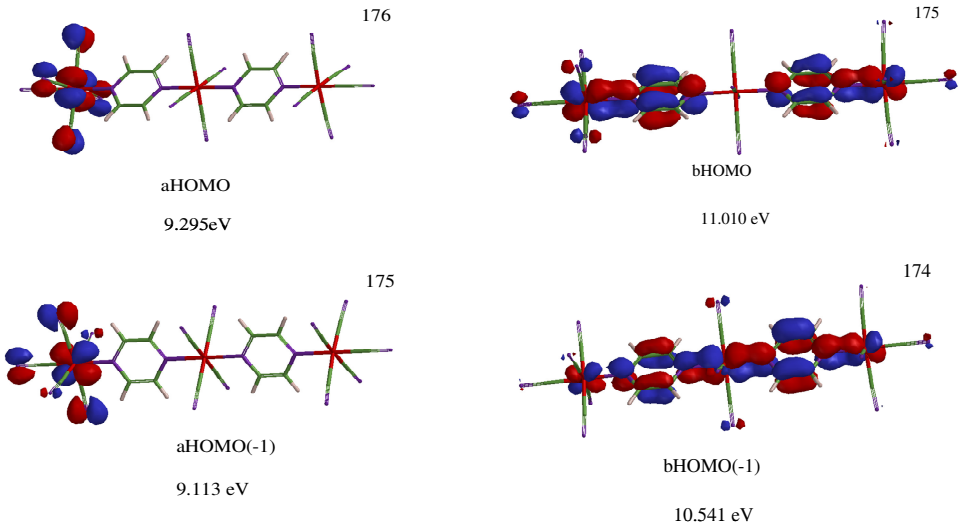

Figure 3.46. HOMO and HOMO(-1) of pyz-tnc(-7)trans complex

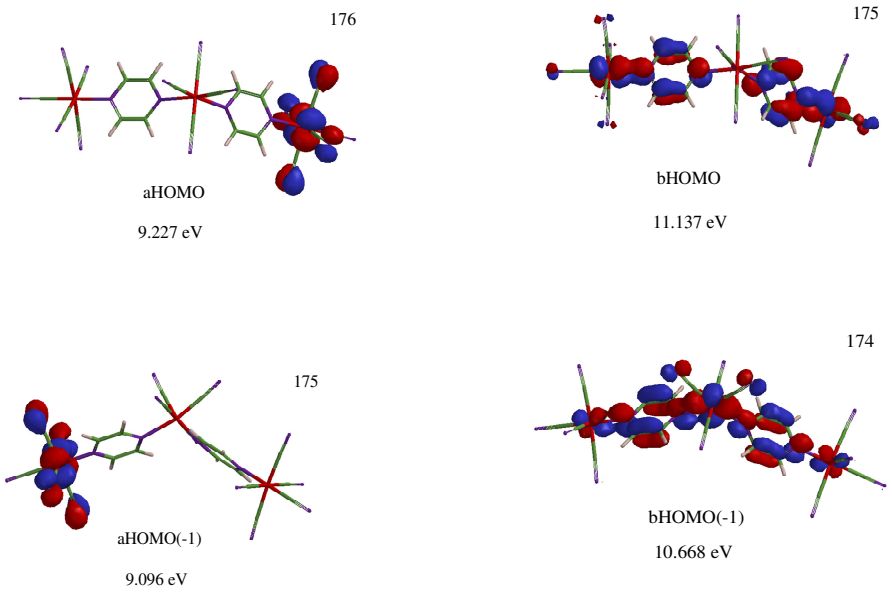

Figure 3.47. HOMO and HOMO(-1) of pyz-tnc(-7)cis complex

Of the trinuclear complexes (-5), (-6) and (-7), the beta-HOMO, beta-HOMO(-1) and HOMO, are of same character for both pyrazine and tetrazine only for tnc(-7). There are the SOMO (index176) on metal frames, beta-HOMO(index 175) which shows π bond over Fe-N bonds on both ends and beta-HOMO(-1)(index 173) π bond over all Fe-N bonds.

Pyz-tnc(-5) (Figure 3.42, 3.43) and pyz-tnc(-6) (Figure 3.45, 3.46) complexes do not have any π bond over Fe- N bonds.Pyz-tnc(-7) (Figure 3.47) complex have π bond over Fe- N bonds. The trends observed in bond lengths are well explained with the presence/absence of the Fe-N π bonds.

The Mulliken charge distributions are shown in Figure 3.48 to Figure 3.50. Ligands are positively charged for pyz-tnc(-5) complexes in Figure 3.48.

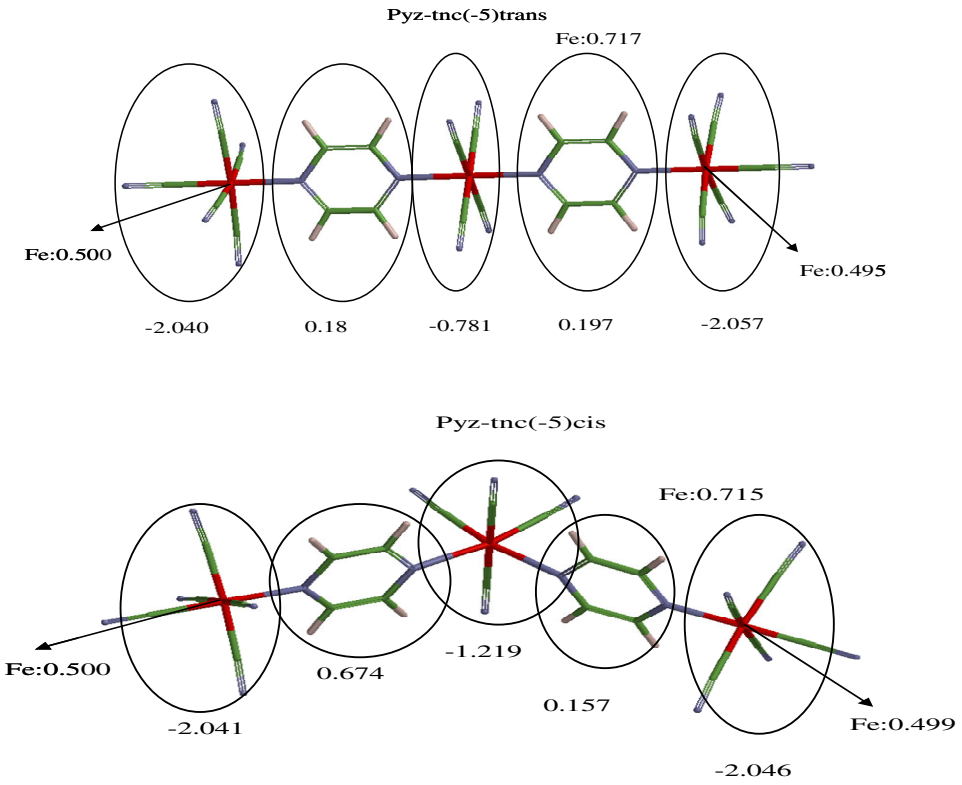

Figure 3.48. Mulliken charges of pyz-tnc(-5)trans and pyz-tnc(-5)cis complexes

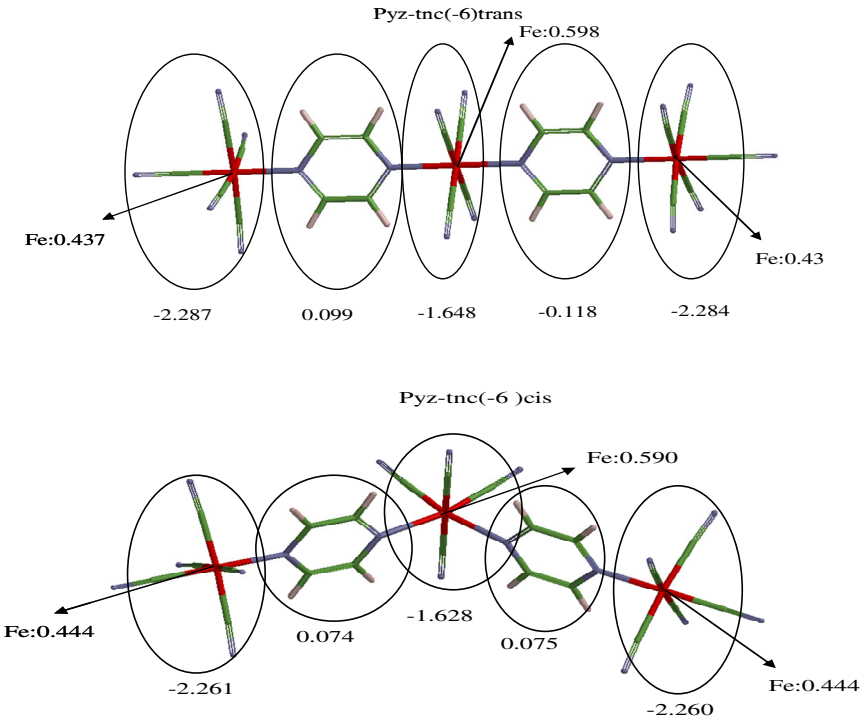

Figure 3.49. Mulliken charges of pyz-tnc(-6)trans and pyz-tnc(-6)cis complexes

In Figure 3.49, it is seen that one ligand becomes negative in trans isomer while both are positive for cis isomer. The trans isomer has 1.97 % of its charge on pyrazine ligand.

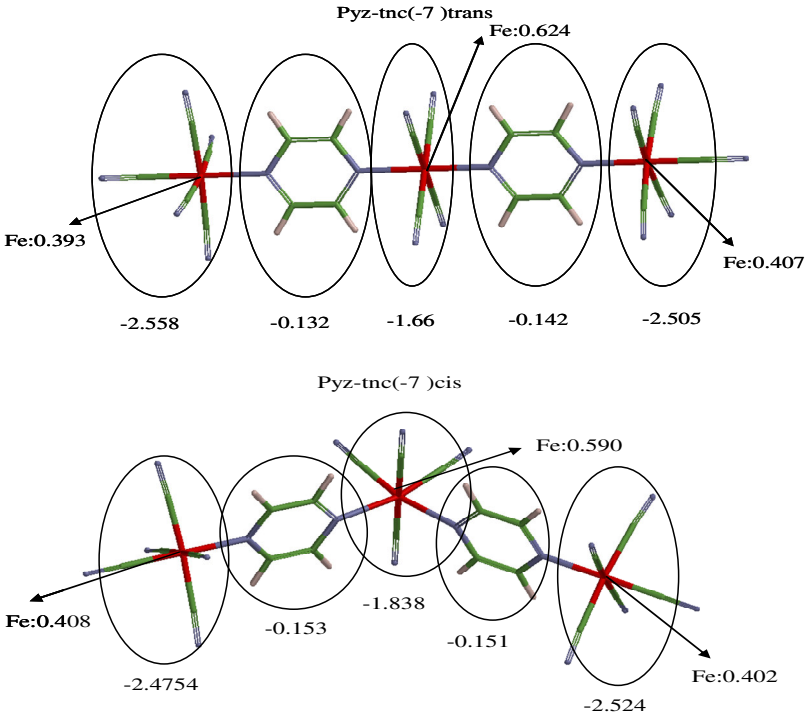

Figure 3.50. Mulliken charges of pyz-tnc(-7)trans and pyz-tnc(-7)cis complexes

Negative charge is observed on pyrazine ligands for pyz-tnc(-7) complexes. Approximately 2 % of the charge is on each pyrazine ligand.

The spin is observed to be mainly on the metal frames for all trinuclear complexes (Figure 3.51 to Figure 3.54)

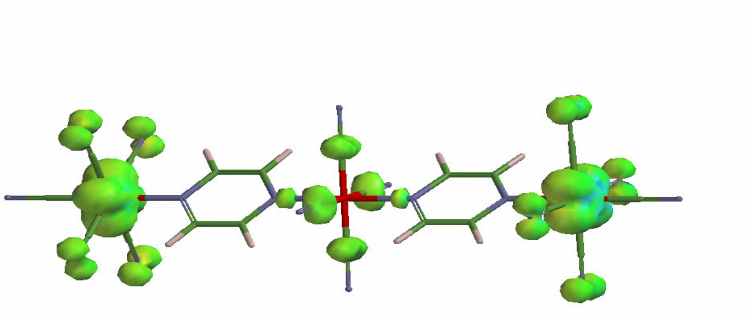

Figure 3.51. Spin of pyz-tnc(-5)trans complex

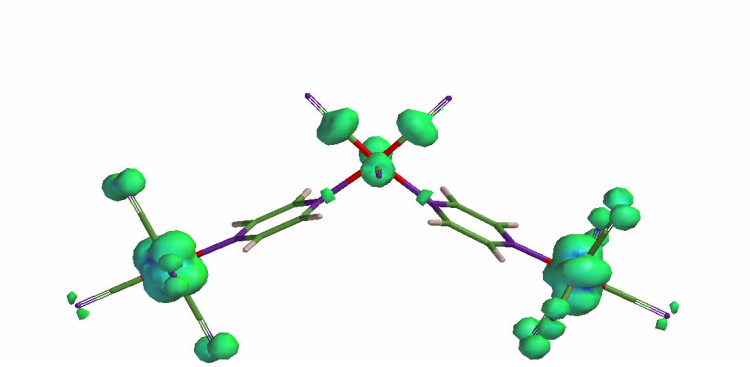

Figure 3.52. Spin of pyz-tnc(-5)cis complex

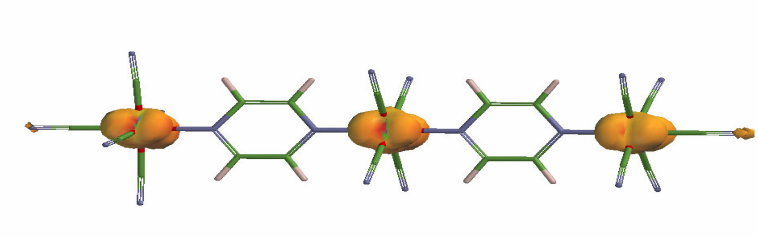

Figure 3.53. Spin of pyz-tnc(-7)trans complex

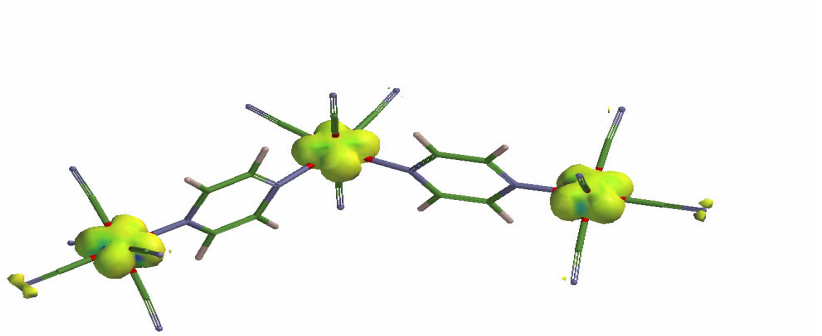

Figure 3.54. Spin of pyz-tnc(-7)cis complex

3.5. PYRAZINE MONO NUCLEAR DILIGAND

The behavior around the middle metal fragment compared to terminal metal fragments urged the modeling of $[L_2Fe(CN)_4]^{1-,2-}$, L=pyz, for completeness purposes (Figure 3.55).

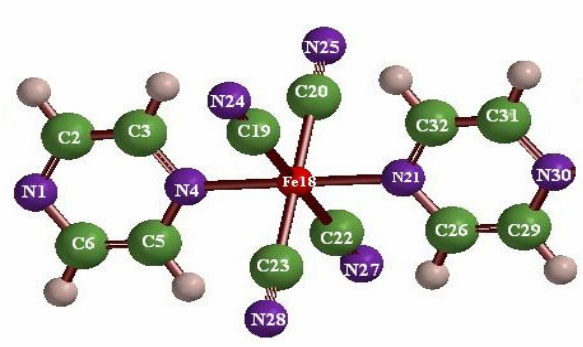

Figure 3.55. Structure and numbering of $[pyz_2Fe(CN)_4]^{1-,2-}$ complexes

Table 3.10. Bond lengths (Å) for pyz-mndl(-1) and pyz-mndl(-2) complexes.

BOND	pyz-mndl(-1)	pyz-mndl(-2)
N1-C2	1.337	1.343
C2-C3	1.393	1.389
C3-C4	1.344	1.351
N4-C5	1.344	1.351
C5-C6	1.393	1.389
N1-C6	1.337	1.343
N1-N4	2.810	2.840
N4-Fe18	2.017	1.972
Fe18-C19	1.963	1.973
Fe18-C20	1.963	1.973
Fe18-N21	2.017	1.972
Fe18-C22	1.963	1.973
Fe18-C23	1.963	1.973
C19-N24	1.169	1.175
C20-N25	1.169	1.175
C22-N27	1.169	1.175
C23-N28	1.169	1.175
N21-C26	1.344	1.351
C26-C29	1.393	1.389
C29-N30	1.337	1.343
N30-C31	1.337	1.343
C31-C32	1.393	1.389
C32-N21	1.344	1.351
N21-N30	2.810	2.840

A comparison of pyz-mndl(-2) and pyz-mndl (-1) bond lengths show that N4-Fe18 and Fe18-N21 bonds shorten while Fe-C bonds lengthen and N1 to N4 and N21 to N30 distance has a net elongation of 0.030 Å on reduction.

Pyz-mndl(-1) has aHOMO, aHOMO(-1), bHOMO and bHOMO(-1) concentrated over the metal fragment.(Figure 3.56)

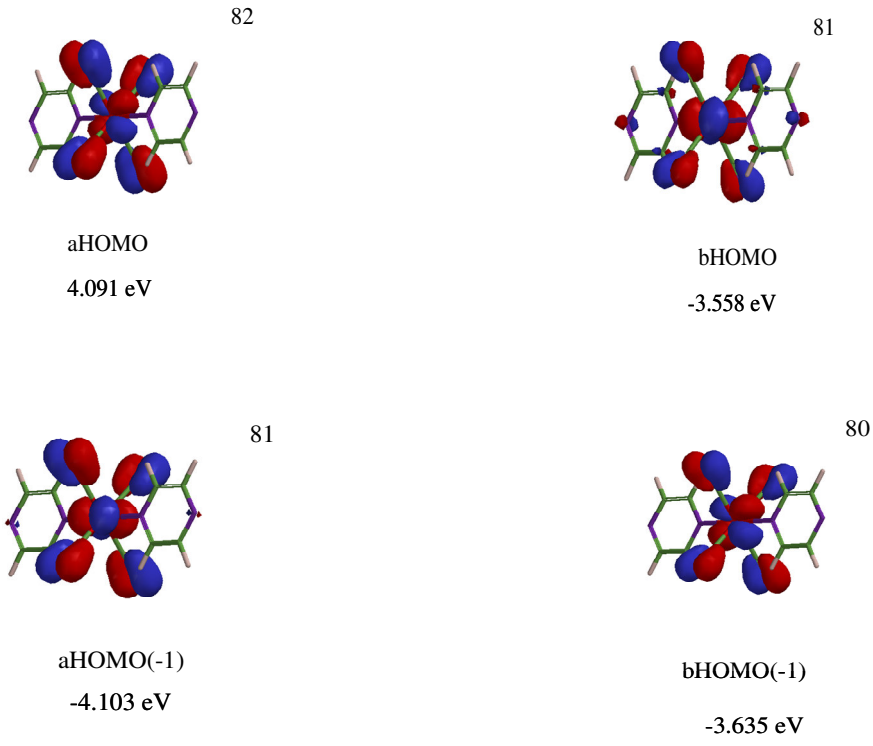

Figure 3.56. HOMO and HOMO(-1) of pyz-mndl(-1)

The HOMO is concentrated over the metal fragment. HOMO(-1) of this complex has π character over the Fe-N bonds.(Figure 3.57)

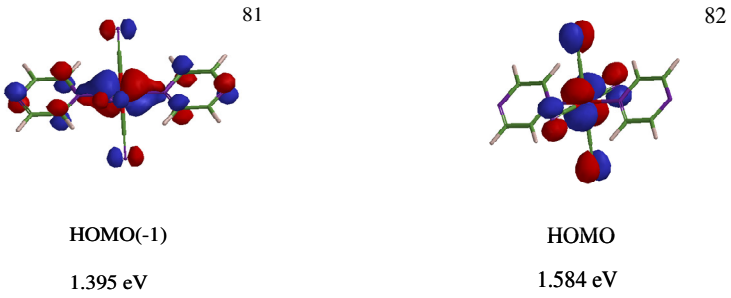

Figure 3.57. HOMO and HOMO(-1) of pyz-mndl(-2)

Charges on ligands are positive for pyz-mndl(-1) complex. The charge percentage per ligand is 4.35 % on pyz-mndl(-2). (Figure 3.58)

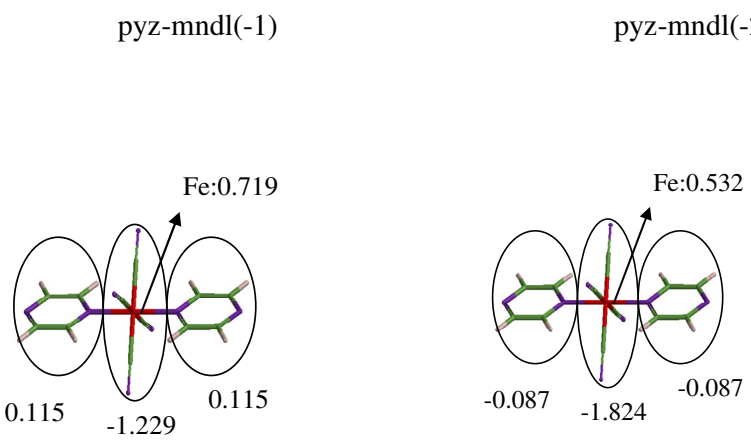

Figure 3.58. Mulliken charges of pyz-mndl complexes

The spin is observed to be on the metal fragment for the complex. (Figure 3.59)

A comparison of pyz-mndl(-2) to pyz-mndl(-1) shows that reduction has caused some charge transfer on the ligand, the Fe-N bond shorten (HOMO(-1) displaying π orbital).

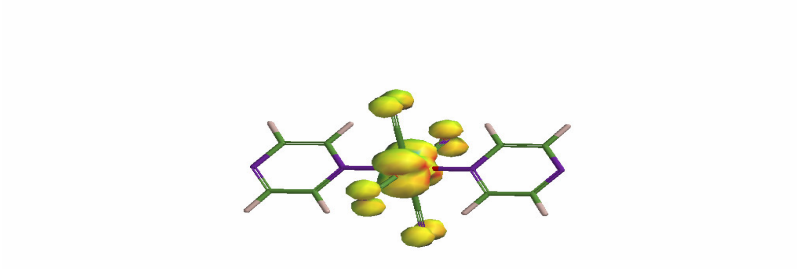

Figure 3.59. Spin of pyz-mndl(-2) complex

The modeling of the central metal fragment with pyrazine ligand show shortening Fe-N bond upon reduction as in trans pyz-tnc(-7). The lengthening of central Fe-N bonds in trinuclear systems for the central metal fragment in pyz-tnc(-5) and (-6) is not exhibited in these systems. (Pyz-tnc(-5) and (-6) complexes do not have Fe-N π bonds.)

4. CONCLUSIONS

Tetrazine has a lower LUMO than pyrazine. Overlap of Fe d orbitals with the ligand tetrazine is easier. In mononuclear complexes, mnc(-2), mnc(-3) tetrazine, one ligand exists per one metal frame. In dnc structures addition of a metal framework (metal of CN-co-ligands) brings more charge on a system with one ligand. Ligand is expected to enrich in charge if there is charge transfer to the ligand. The ligand donates electrons to form the Fe-N σ bond and than accepts back electrons into its π^* orbital through the Fe-N π bond observed in frontier orbitals.

Of the mnc(-2) complexes the one with tetrazine ligand has negative charge whereas the one with pyrazine ligand has positive charge. Of mononuclear complexes, mnc(-3) have shorter Fe-N bonds due to π bonding between the Fe d orbital and the ligands' π^* orbital. The ligand tetrazine has higher negative charge percentage compared to pyrazine. Spins for mnc(-2) complex shows spin on tetrazine ligand but none on pyrazine ligand. Comparing the dnc complexes, pyz-dnc(-4) has positive charge on ligand, tetrazine-dnc(-4) has negative charge with some MLCT . Upon reduction both dnc complexes have negative charges on ligand with charge percentage on tetrazine being almost twice the amount observed on mnc.

Spins of dnc show some spin on ligand tetrazine but none on pyrazine.

Results of calculations show that tetrazine having lower LUMO is a better acceptor of electron compared to pyrazine. Tetrazine leads to higher MLCT in mnc, dnc and tnc species.

Tnc(-5) and tnc(-6) of tetrazine have Fe-N π bonds which are not observed for tnc(-5) and tnc(-6) of pyrazine. Therefore trends in bond lengths upon reduction do not follow the same pattern.

Tz-tnc(-5) and tz-tnc(-6) have negative charges on ligands which indicate formation of delocalization on the ligand. Pyz-tnc(-5) has no negative charge on ligand, tnc(-6) has some negative charge on the ligand.

Spin on tnc for pyrazine are detected only on metal frames. Spins on tnc for tetrazine, in contrast to pyrazine, are observed both on ligands and metal frames. Tnc(-7) for both tetrazine and pyrazine have similar frontier orbitals with tetrazine having more charge on ligand.

REFERENCES

1. Prassides, K., “Mixed Valency Systems-Applications in Chemistry, Physics and Biology”; Kluwer Academic Publishers; Dordrecht, 1991.

2. Taube, H., “Electron Transfer between Metal Complexes-in Retrospect (Nobel Lecture)” Angew. Chem. 1984, 23, 329-338.

3. Kaim, W., A. Klein and M. Glockle, “ Exploration of Mixed-Valence Chemistry: Inventing New Analogues of the Creutz-Taube Ion”, Acc.Chem.Res., 33(2000)755-763.

4. Bencini, A., I. Ciofini, C.A.Daul and A. Ferretti, “Ground and Excited State Properties and Vibronic Coupling Analysis of the Creutz-Taube Ion, $[(NH_3)_5Ru\text{-pyrazine-}Ru(NH_3)_5]^{5+}$, Using DFT” J.Am.Chem.Soc.1999, 121, 11418-11424.

5. Dunbar, K. R. and R.A.Heintz, ”Chemistry of Transition Metal Cyanide Compounds: Modern Perspectives“ Prog. Inorg. Chem. 1997, 45, 283-391.

6. Creutz, C., ”Mixed-Valence Complexes of d^5-d^6 Metal Centers” Progr. Inorg. Chem. 1983, 30, 1-73

7. Creutz, C. and H.Taube, “Binuclear Complexes of Ruthenium Ammines.” J. Am. Chem. Soc. 1973, 95, 1086-1094.

8. H.E. Toma and J.M. Malin, Inorg. Chem., 12, 1039 (1973)

9. R. E. Shepherd, J. Am. Chem. Soc., 98, 3329 (1976)

10. Felix, F. and A.Ludi, ” Mixed-Valence Properties of Ligand-Bridged Iron-Cyano Complexes” Inorg. Chem. 1978, 17, 1782-1784.

11. Ketterle, M., W.Kaim, J.A.Olabe, A.R.Parise and Fiedler, J., "Widely Differing Stabilities of Molecule_Bridged Cyanodiiron(III,II) Species in Non-Aqueous Solvents" Inorg. Chim. Acta 1999, 291, 66-73.

12. Sonja B.Braun-Sand and O.Wiest, J.Phys.Chem 107(2003) 285-291.

13. Ernst. S., V.Kasack and W.Kaim, Inorg. Chem. 1988, 27, 1146.

14. Glockle, M., J.Fiedler, N.E. Katz, M.Garcia Posse, E. Cutin, and W. Kaim, "The Fe^{III}/Fe^{II} vs $Fe_2^{2.5}$ Formulation in Mixed-Valent Species $[(NC)_4Fe(BL)Fe(CN)_4]^{3-}$, BL=2,2`-Bipyrimidine and 3,6-Bis(2-pyridyl)-1,2,4,5-tetrazine. Distance and Size Do not Always Matter" Inorg. Chem. 1999, 38, 3270-3274.

15. Gafney, H. D., T. C.Strekas, A. P.Baker and C. H.Braunstein, Inorg. Chem. 1984, 23, 857.

16. Brewer, K.J., Jr.W.R.Murphy and J.D.Petersen, "Synthesis and Characterization of Monometallic and Bimetallic Mixed-Ligand Complexes of Iron(II) Containing 2,2'-Bipyridine or 2,3-Bis(2-pyridpyl)pyrazine" Inorg. Chem.1987, 26, 3376-3379.

17. Glöckle, M. and W. Kaim, "An Exceedingly Stable Mixed –Valent Diiron –(II,III) Complex Ion $\{(tz)[Fe(CN)_5]_2\}^{5-}$ with Comproportionation Constants Between 10^8 (in H_2O) and 10^{19} (in CH_3CN)" Angew. Chem., Int. Ed. Engl. 1999, 38, 3072-3074.

18. Glocke, M. W. Kaim, A. Klein, E.Roduner, G. Hübner, S. Zalis, J .Van Slager, F.Renz and P. Gütlich, "The Stable Diiron(2.5) Complex Ion $[[CN)_5Fe(\mu\text{-}tz)Fe(CN)_5]^{5-}$, tz=1,2,4,5-Tetrazine, and Its Neighboring Oxidation States" Inor.Chem 2001, 40(2001)2256-2262

19. SPARTAN'04 for Windows 1.03, Wavefunction, Inc.18401, Von Karman Ave., 370 Irvine, CA 92715 USA. © 2004 Wavwfunction, Inc.

20. Handy, N.C., "Density Functional Theory", in: B. O. Roos (ed.), Lecture Notes in Quantum Chemistry, Vol. 2, pp. 91-123, Springer-Verlag, Berlin, 1994.

21. Becke, A. D., "Density Functional Thermochemistry. III. The Role of Exact Exchange", J. Chem. Phys., Vol. 98, pp. 5648-5652, 1993

22. Lee, C., W. Yang and R.G. Parr, "Deveopment of Colle-Salvetti Correlation Energy Formula into a Functional of the Electron Density", Phys. Rev. B, Vol. 37, pp. 785-789, 1988

23. Fernandes, M. A., V. Circu, R. Weber, T. Varnalı and L. Carlton, "Tris(triphenylphosphine)rhodium Cyano and Triphenylcyanoborate Complexes: Structures and a DFT study", Journal of Chemical Crystallography, Vol.32, pp.273-285, 2002.

24. Koch. W. and M.C. Holthausen, "A Chemist's Guide to Density Functional Theory" Second Edition, pp. 82.